Nanoscale

Rare-earth-free high energy product manganese-based magnetic materials

Journal:	*Nanoscale*
Manuscript ID	NR-REV-03-2018-001847.R1
Article Type:	Review Article
Date Submitted by the Author:	28-May-2018
Complete List of Authors:	Patel, Ketan; University at Buffalo - The State University of New York Zhang, Jingming; University at Buffalo - The State University of New York Ren, Shenqiang; University at Buffalo - The State University of New York

Nanoscale

ARTICLE

Rare-earth-free high energy product manganese-based magnetic materials

Received 00th January 20xx,
Accepted 00th January 20xx

DOI: 10.1039/x0xx00000x
www.rsc.org/

Ketan Patel,[a,b] Jingming Zhang,[a,b] and Shenqiang Ren[a,b,*]

ABSTRACT: The constant drive to replace the rare-earth metal magnets has initiated a great interest for an alternative. Manganese (Mn) has emerged to be a potential candidate as a key element in the rare-earth-free magnets. Its five unpaired valence electrons give it a large magneto-crystalline energy and the ability to form several intermetallic compounds. These factors have led Mn-based magnets to be the potential replacement for the rare-earth permanent magnets for several applications like efficient power electronics, energy generators, magnetic recording and tunneling applications, and spintronics, etc. For past few decades, Mn-based magnets have been explored in many different forms such as bulk magnets, thin-films, and nanoparticles. Here, we review the recent progress in the synthesis and the structure-magnetic property relationships of Mn-based rare-earth-free magnets (MnBi, MnAl and MnGa). Furthermore, we discuss their potential to replace the rare-earth magnetic materials through the control on their structure and composition to achieve the theoretically predicted magnetic properties.

1. Introduction

Permanent magnets (PMs) are an integral part of the modern world which are indispensable in many critical technologies, including power electronics, transformers, high energy-product motors and generators, as well as medical equipment[1-4]. However, managing the cost and environmental footprint of scalable magnet growth becomes a growing challenge, particularly rare-earth (RE) based PMs. Furthermore, current state-of-the-art PMs with continuously growing demand closely rely on RE elements (Nd/Sm/Dy/Pr/La), and such strategic and insecure sources have raised severe concerns due to their availability, extraction difficulties and national securities[5-9]. This has triggered significant efforts in magnetic metal community to develop new alternative magnetic materials consisting of RE-free elements. Although the theoretically predicted value of the BH_{max} for RE-free magnetic material is less than that of the RE magnetic materials, the enormously less hazardous nature of RE-free magnetic materials provides us the motivation essential to invest our efforts into discovering more and more RE-free magnets. Prospective candidates with high earth abundance, such as Fe/Ni/Mn, constitute of critical strategic materials for RE-free superior magnets. In this context, strong motivations exist to drive the development of next-generation RE-free PMs which are lightweight, high energy product, mechanically machinable and corrosion resistant[3, 10-16].

Manganese forms a vast variety of intermetallic compounds due to its half-filled valence shell. The unpaired electrons also make it a highly magnetically active material with intrinsic magnetic moment. In addition, Mn element is abundant in the Earth's crust and it is inexpensive to process when compared to the RE elements. Among the known intermetallic compounds, Mn-based MnBi, MnAl and MnGa, are few of the most common alloys that have been studied as potential replacements for the RE magnets[17-29]. Low-temperature phase MnBi alloy has shown the highest energy product (16.2 MGOe) among the three, whereas the low-cost MnAl alloy ($4/kg) is readily machinable and possesses a high modulus of elasticity[27-29]. The MnGa alloy falls in the between MnBi and MnAl regarding the performance and cost, which performs better than that of MnAl and is cheaper than MnBi as Ga (.0019%) is more abundant than Bi (2.5×10^{-6}%) in the Earth's crust. For decades, much effort has been made to understand the mechanism, structures, and magnetic properties of these Mn-based magnets. This review summarizes the latest advancements in Mn-based magnetic alloys across different dimensions, with the aim to further push the boundary for this dynamic and critical subject. In the following, the development of MnBi, MnAl and MnGa alloys is discussed, containing their synthetic techniques, and structural and magnetic properties.

2. Structure and magnetic properties of MnBi magnetic materials

After decades of scientific research, MnBi has emerged as one of the rare-earth-free permanent magnets. As a promising alternative for the rare-earth magnets (such as Nd-Fe-B magnets), MnBi possess great magnetocrystalline anisotropy (1.6×10^{6} J m^{-3}), which depends on several parameters discussed in this section. One of the key features that makes MnBi a unique permanent magnet is that its coercivity has a positive temperature coefficient. In other words, unlike the regular tendency, the coercivity of MnBi tends to increase with the rise in the temperature. A broad bifurcation shows that MnBi permanent magnets exist in three different forms - bulk, thin-films, and nanoparticles. The existence of MnBi in each of

[a] *Department of Mechanical and Aerospace Engineering, University at Buffalo, The State University of New York, Buffalo, NY 14260*
[b] *Research and Education in eNergy, Environment & Water (RENEW) Institute, University at Buffalo, The State University of New York, Buffalo, NY 14260*

these forms and their magnetic properties are majorly dependent of its synthetic methods. Despite many reported scientific work, there are still efforts being made to reach the theoretical value of the energy product of the MnBi that is around 18 MGOe[30].

2.1 MnBi Bulk Magnets

Among all the existing phases of MnBi, the low-temperature phase (LTP) is the one of interest as this is the phase that possesses the high magnetocrystalline anisotropy. As the name suggests, the LTP exists when the synthesis of MnBi takes place under 340 °C. A significant amount of effort has been put into the synthesis of the MnBi bimetallic complex that has larger weight percentage of LTP phase, which in turn contributes towards a higher energy product of the final product. However, the magnetocrystalline anisotropy is not the only parameter dictating the energy product of a magnet, and a linear relationship between the two parameters has not been seen [21, 31-36].

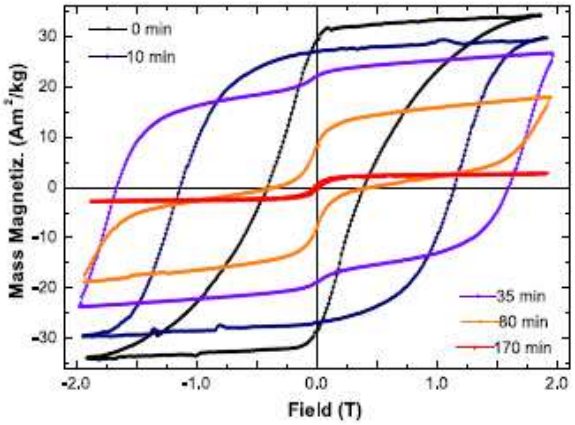

Figure 1. Magnetic hysteresis loops of MnBi with the magnetic field applied parallel to the direction of the aligned powder under various ball milling times, from 0 to 170 min. Republished with the copyrights from [42].

The primary challenge in the synthesis of the high-quality MnBi arises due to the preparation of a highly rich LTP-MnBi. There are several factors responsible for the challenge, such as the vast difference in the melting points of Mn and Bi. However, the most fundamental one is the peritectic reaction between Mn - Bi around 355 °C. Mechanochemical method, melt-spinning, sintering, wet chemistry are some of the ways utilized to prepare the LTP-MnBi[32, 35, 37-41]. However, none of these methods seem to successfully form the crystallographically anisotropic MnBi particles. In order to obtain a highly pure MnBi, Kanari, et al. addressed this challenge through a surfactant-assisted high-energy ball milling process[42]. The MnBi ingot, prepared via arc-melting, was subjected to a time-dependent (1, 2, 3, 5, 10, 20, 40 and 80 h) surfactant assisted high energy ball-milling (SEHEBM) and their effect of the structure and the magnetic properties were studied. In addition, the effect of the ambient atmosphere on the MnBi particles was also recorded. It was found that after SEHEBM, the sample had 82.6% LTP-MnBi, 12.7% Bi and 4.8 Mn with the atomic ratio between Mn and Bi being 50:50 and a minimum particle size reaching close of 500 nm after an hour of milling, showing a saturation magnetization (Ms) around 75 $Am^2\ kg^{-1}$ (Figure 1). The size remained nearly constant for the rest of the milling time. The atomic ratio was altered by the SEHEBM for over 2 hours of milling from $Mn_{50}Bi_{50}$ to $Mn_{40}Bi_{60}$, which kept reducing to $Mn_{35}Bi_{65}$ after 80 hours of SEHEBM. The rationale behind the variation in the atomic ratio is yet to be discovered. This demonstrates the high sensitivity of the MnBi towards the high energy ball-milling and the destruction of the LTP. In addition, after the SELEBM process, the particle size was around 3.5 µm after 10 minutes of milling time, which then further reduced to 1 µm after 170 min of milling time. Furthermore, it was important to note the consistency of the 50:50 atomic ratio for all the SELEBM. There is almost no ferromagnetism for the sample milled for 170 min and this could be due to the surface oxidation and the particle size getting smaller than the single domain size (500 nm), as shown in Figure 1. This method for preparing LTP-MnBi can serve a key role in enhancing the efficiency towards the synthesis of high energy product MnBi. Furthermore, the same technique can also be applied for other magnetic alloys with some modifications based on their phase diagrams. Additionally, reducing the Bi and Mn content from initial Mn-Bi ingot can further maximize the potential of this technique.

Another attempt to maximize the energy density was based on the prediction of Kneller and Hawig[43], Nguyen et al. attempted to synthesize an exchange coupled hard/soft magnetic complex by combing magnetically hard MnBi with the soft Co nanowires (NWs)[44]. The MnBi alloys were prepared by arc melting Mn and Bi at 1:1 ratio and annealing the as-prepared ingot at 300 °C under Ar protection by using a specific temperature profile (discussed in a later section). Reference [45] was followed to synthesize the Co NWs. Finally, the MnBi was ground and mixed with appropriate weight ratios of Co NWs. The mixture was then subjected to a cryo-ball milling under the liquid N_2. The mixture was then compacted at 300 ^oC under 2000 psi in an aligning field of 18 kOe. The magnetic properties were dictated by optimizing the Co NWs, and therefore, a lot of effort has been made to optimize the reaction temperature and time for the synthesis of Co NWs. The maximum energy product achieved by this method was 4.8 MGOe at room temperature. As discussed in the earlier section, the wt% of the LTP-MnBi is one of the key parameters responsible for obtaining high energy product. Due to the large difference in the melting points of Mn and Bi, a complete formation of the LTP-MnBi has not yet been possible. This is also followed by some percentage of unreacted Mn and Bi, which contributes negatively towards the magnetic properties of the bulk magnet[30, 46]. Hence, several different strategies have been reported for the enhancement of the LTP MnBi. For example, in 2014, Nguyen et al. reported a specific temperature profile for sintering the MnBi ingot, which would improve the LTP content in the final product[47]. Another research reported a high content LTP-MnBi formation via melt-spinning technique. In the case of the LTP enhancement via profile heat treatment (PHT), the MnBi alloy was prepared by arc-melting Mn and Bi at 1:1 ratio three times to ensure the homogeneity of the alloy[47]. The alloy was then subjected to the PHT and then milled in air with the particles size being as large as 150 µm. The powder was used to make bulk magnets for further analysis. The PHT consists of four stages, which composed of a high-temperature heating stage followed by three different steps of cooling, as seen from the Figure 2. During the stage 3, the cooling rate is .1 ^oC/min, and considered as a "pseudo-equilibrium solidification

process", which enhances the formation of LTP-MnBi. The following reaction shows the formation of the LTP from the HTP between the stage 2 and stage 3.

$$\alpha 1MnBi(HTP)+\beta 1Mn+\beta 1Bi \rightarrow \alpha 2MnBi(LTP)+\beta 2Mn+Bi^{*} \quad (1)$$

Here, Bi* refers to the Bi stuck on the surface of annealing boat and the solidified Bi spheres on the surface of the MnBi alloy after the third stage. Removing the Bi-rich top layer and conducting the Rietveld Refinement analysis showed the average LTP content close to 94 wt% of the total MnBi composite. Furthermore, the LTP MnBi + Mn composite showed the maximum energy product of 6.1 MGOe and the saturation magnetization being close to 73 emu/g. To further enhance the energy product of the MnBi permanent magnet, it has been reported the preparation of a high LTP (~90%) content MnBi by melting highly pure Mn and Bi and then forming Mn-Bi ribbons via melt-spinning under Ar protection. The ribbons were then sintered at 300 °C and the annealed product was then crushed and milled. To make a bulk magnet, the green-compacts were subjected to hot compaction at 300 °C for about 4 minutes with the applied pressure being 300 MPa. In this technique, the melt-spinning distributed the Mn and Bi homogenously, which subsequently, gave a high LTP content after the annealing. Furthermore, among three different weight ratios, the highest LTP was observed in $Mn_{52}Bi_{48}$. The LTP intensity in the XRD analysis was reduced by the increase of Bi weight ratio (Figure 3). Also, the temperature-dependent energy product was the maximum, 6.7 MGOe, at the room temperature. The value decreased to 5.5 MGOe as the temperature elevated to 150 °C. Furthermore, in a study conducted by Nguyen et al. to understand the LTP formation, it was found that the particle size of the phases ($Mn_{50}Bi_{50}$, Mn and Bi) present in the MnBi composite depended on the cooling rate [48]. Faster cooling rates tended to form smaller grains with a possibility of attaining an amorphous phase at a cooling rate ~106 °C/s. This is important as the coercivity, a key parameter for obtaining high energy product, depends on the grain size. It was found that the evolution of LTP followed 1-D time-dependent diffusion equation. The detailed discussion of the LTP evolution can be found in the ref [9]. The cooling rate of the MnBi alloy was controlled by the alloy mass of 1g, 3g and 4g, and the obtained microstructure showed the grain sizes of 2 µm, 6 µm and 10 µm (Figure 4), respectively. The X-ray diffraction for the optimum LTP content was observed in the sample with the grain size of 2 µm. Therefore, it was then annealed for 12 hours at 280 °C and ball-milled to make a high LTP content bulk magnet. To do so, the milled powder was aligned under 18 kOe of magnetic field followed by a compaction under an applied pressure of 12 MPa. The green-compact was then rapidly heated to 280 °C under Ar atmosphere for 10 minutes that resulted in a permanent magnetism with a maximum energy product of 7.0 MGOe. However, the maximum energy density reported for MnBi bulk magnets is 8.4 MGOe. This number was achieved by preparing the bulk magnet consisting of a very high LTP content (96 wt%), which was synthesized by subject the arc-melted ingot to cycles of grinding and sintering in vacuum at 300 °C. Furthermore, the optimized sample consisted of 1-7 µm sized particles, with coercivity around 12 kOe, that were obtained after subjecting the milled powder to a low temperature (-120 °C) ball milling. The low temperature and the duration of milling (150 min) aids in maintaining a proper balance among $_{i}H_{c}$, LTP and M_{s} of the particles. Finally, the powder was subjected to the warm compaction under 200 MPa at 245 °C for 30 minutes. The bulk magnet was aligned under a magnetic field of 20 kOe. In this case, the high energy product is very much dependent on the quality of the initial MnBi alloy as it was subject to several cycles of milling and sintering. Also, the large applied pressure and the larger aligning magnetic field also played important roles in approaching 8.4 MGOe.

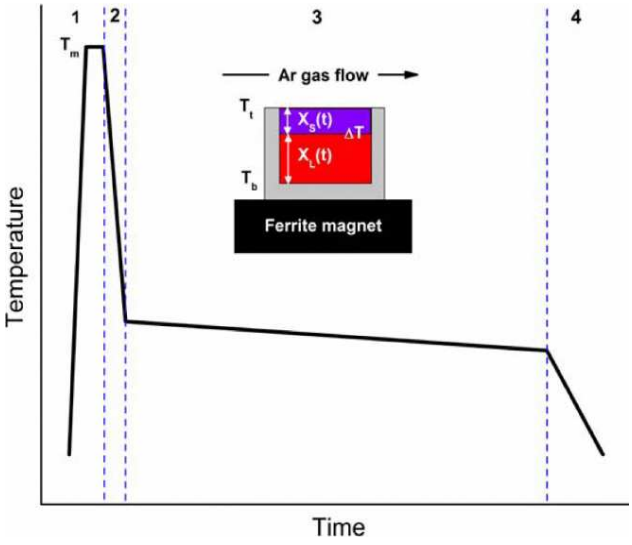

Figure 2. Temperature profile used for the PHT of magnetic MnBi alloys. Inset: The scheme of the alloy in the cylindrical ceramic boat placed onto the ferrite magnetic substrate. 1, 2, 3, and 4 denote the stages of the heat treatment. Republished with the copyrights from [47].

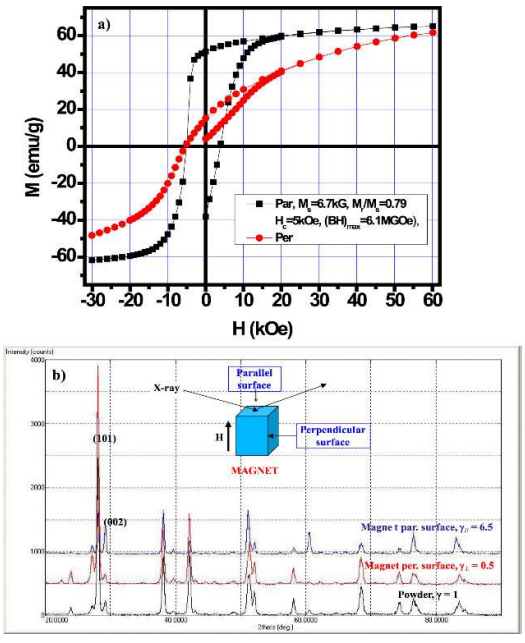

Figure 3. (a) Magnetization loops of MnBi magnet measured with the parallel (black curve) and perpendicular (red curve) orientations to the magnet alignment direction. (b) XRD patterns taken from both parallel and perpendicular directions of the magnet. Republished with the copyrights from [47].

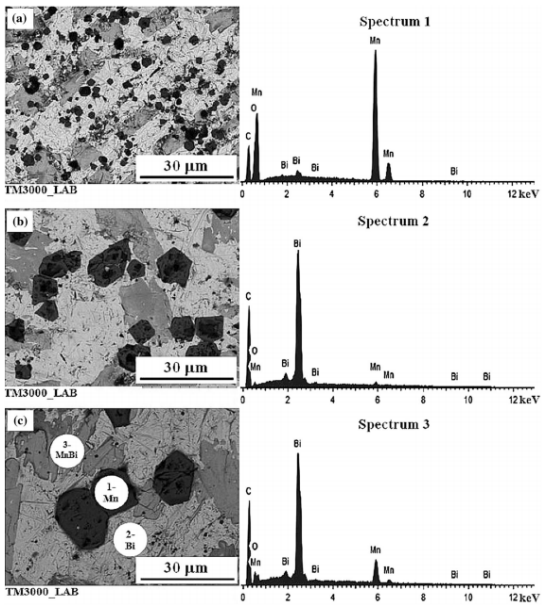

Figure 4. The microstructures of MnBi arc-melted alloys with the different alloy masses 1 g (a), 3 g (b), and 8 g (c). The EDX spectra 1, 2 and 3 were taken at the points 1, 2 and 3 which are marked on Fig. 1c. Republished with the copyrights from [48].

2.2 MnBi thin films

The first ever reported preparation of the MnBi thin-film permanent magnets was in 1957 by Williams et al., [49] in which Mn and then Bi layer was deposited on a glass substrate and then vacuum annealed for three days in the temperature range of 225 - 350 °C. Their large uniaxial anisotropy with easy "c" axis, large Faraday rotation and a large saturation magnetization at room temperature have made the α-MnBi thin films (LTP-MnBi) a rare-earth-free magnetic material for several applications such as high-density recording, magneto-optic applications, magnetic storage and erasable magnetic holography applications. Furthermore, the α-MnBi (NiAs structure) into its high-temperature phase (HTP) β-MnBi with a distorted Ni2I structure over 360 ˚C[50, 51]. Quenching the HTP gave a meta-stable quenched high-temperature phase (QHTP) that is even better for the above-mentioned applications. However, the long-term stability of the QHTP has always been a challenge [52-54]. Hence, a lot of effort has been made for past few decades to understand the thin-film growth with a high LTP content and to stabilize the QHTP-MnBi[52, 55, 56].

In 1971, the preparation and stability of MnBi thin-films on various substrates was reported to illustrate the effects of the substrates on the growth of the lattice of the MnBi[56]. This work demonstrated the stability of the HTP at room temperature and the fabrication of uniform and large-area (15 in^2) MnBi thin films. According to this work, among several different substrates, mica turned out to be the best substrates for the high-quality film growth. This is due to the similarity between the basal planes of the mica and the MnBi. However, mica being optically biaxial, it failed to meet the criteria from the device point of view. It is a noteworthy detail that depositing Bi as the first layer is a crucial factor in forming a high-quality MnBi thin film. This is because the rhombohedral basal planes of Bi grow parallel to the substrate, as stated in the "law of rotation of indices". On the other hand, a first layer of Mn would grow randomly due to its complex crystal structure, resulting in a poor MnBi thin films. The significance of depositing Bi as the first layer was further highlighted from the large difference between melting points of Bi and Mn. The other important finding was the necessity of the addition of excess Mn during the film growth. The excess Mn was required to compensate the Mn that, possibly, got oxidized during the synthesis even though the film was more stable in ambient conditions than its bulk counterpart. The extra stability in the thin film was due to the slower oxidation in the "c" direction.

After the demonstration of the preparation of the MnBi thin films, there arises a need to understand the film formation to optimize the film growth for a better performing QHTP-MnBi thin film. Therefore, Myagkov et al. studied the solid-phase transformations in Mn-Bi system [53, 57]. Research has shown that LTP-MnBi converts into HTP-MnBi at 390 °C, following the reaction

$$\alpha \rightarrow \beta + \mathrm{Bi} \qquad (2)$$

Several researchers have shown that QHTP has an excellent, and better than LTP-phase, magneto-optical properties[52, 55, 56]. However, the QHTP-phase, being metastable, turns back into its LTP-phase over a course of two years, thus, limiting its longevity for the practical implementation[52-54].

$$[\mathrm{QHTP\text{-}Mn1.08Bi} \rightarrow \alpha\text{-}\mathrm{MnBi} + \mathrm{Mn}] \qquad (3)$$

A research group demonstrated the formation of a third, indefinite metastable, phase of MnBi by doping a small amount of Ti in the Mn-Bi system, which formed $Mn_{1-x}Ti_xBi$ stoichiometry. However, the work demanded a better analysis on the LTP-phase of the Mn-Ti-Bi complex. To understand this, Myagkov et al., in 2016, studied the phase transformation in the Mn-Bi system[57]. They began their study by preparing two different thin-films, Mn/Bi (Mn over Bi) and Bi/Mn (Bi on Mn), by thermal deposition method at 1:1 molar ratio. The process was undertaken on two different substrates, glass and pyro Ceram, in a vacuum of 10-6 Torr. Firstly, studying the Mn/Bi sample, all the data from XRD, VSM and the electron microscopes suggested a proper LTP formation. Furthermore, the data from the electron microscopy and the linear energy dispersion X-ray (Figure 5) showed the proper mixing of Mn and Bi layers after the annealing, which was at a maximum temperature of 300 °C. However, it was contrasting to find that the Bi/Mn sample remained non-magnetic till 400°C of annealing process. This could be due to the poor mixing between Bi and Mn layers. Since the Mn layer was deposited first, it is very likely that it suffered a certain amount of oxidation. Also, the large melting temperature gap between Mn and Bi would restrict the liquid of Bi, at 673 K, to diffuse into the Mn layer at that temperature. Also, the asymmetric mixing of Bi into the Mn layer may also be caused due to the kinetic energy barrier for the atomic mixing at the Mn-Bi interface being less than the local acceleration for the Bi atoms being deposited onto the interface. As a conclusion of the work, it is evident that solid phase synthesis of α-MnBi largely depends on the sequence of Mn and Bi deposition.

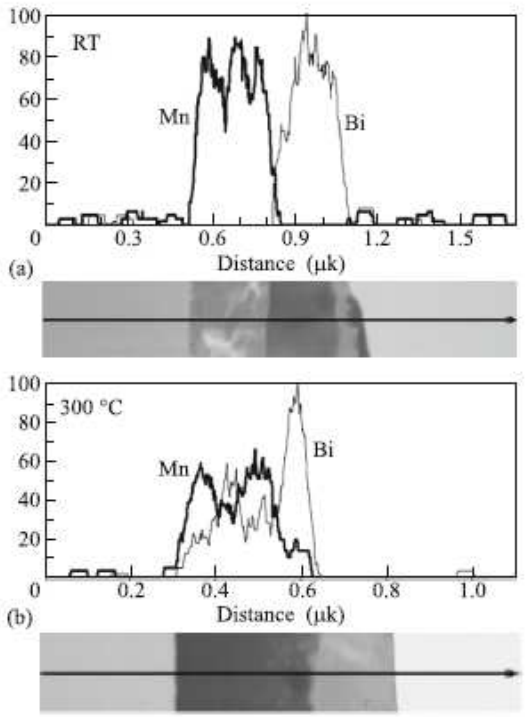

Figure 5. Transmission electron microscopy image and linear scans of energy dispersion X-ray (along the black line) along the cross-section of (a) the initial Mn/Bi (Mn on Bi) sample and (b) the sample annealed at 300°C. Republished with the copyrights from [57].

The desire to enhance the magnetocrystalline anisotropy of the MnBi thin films has been the driving force for the researchers to try various techniques to grow high-quality films, such as magnetron sputtering, e-beam evaporation and molecular beam epitaxy. One such technique, to prepare the highly-textured MnBi thin-films, is via the pulsed laser deposition (PLD) method. It is a widely used technique and several other magnetic thin-films such as NdFeB and FePt have been successfully prepared via this method[58-65]. An important feature of the PLD is that it allows the thin-film preparation at temperatures as low as room temperature. Following this method, Zhou et al. reported the preparation of highly textured MnBi thin films[41]. The film growth was carried under a vacuum of 5 x 10^{-8}Torr with KrF excimer laser (λ = 248 nm) as the source on a glass substrate. The rotation of the substrate ensured the uniformity of the film and the number of pulses dictated the film thickness. Increasing the film thickness showed better crystalline texture along the c-axis. Taking a look at the SEM image (Figure 6), it makes it evident that the Bi layer is crucial for the growth of the textured MnBi and the column-like structures consists of many MnBi grains that are in the nanometer scale. This is because the Bi layer acts as a template for the MnBi growth in the c-direction[41, 57, 66, 67]. On the other hand, depositing Mn as the first layers was met with a couple of major obstacles. First, it required more power from source for the deposition of the Mn layer, as the melting point of Mn is much higher than that of the Bi (Mn = 1244 °C; Bi = 271.3 °C). Secondly, there was no observable phenomena of the preferential growth in the Mn thin film. Hence, the Bi layer turns out to be the better selection. Furthermore, annealing temperature played an important role to bring out the texture and enhance the magnetic properties of the MnBi. The films annealed between 340 °C and 350 °C showed the highest MnBi intensity under the XRD. The peak starts to plummet as the temperature reaches to 360 °C. Hence, the parameters to optimize the thin film included a 200 nm Bi as the first layer and 350 °C annealing temperature. The Rietveld Refinement shows 85 wt% of the LTP-MnBi phase. This number is much lower than the values discussed in the bulk section because of the presence of the additional Bi in the Bi first layer. Furthermore, the oxidation of Mn is also a possibility as discussed in the previous section. When examined for its magnetic anisotropy, the MnBi thin film showed large coercivity (15 kOe) at room temperature, which further increased up to 25.3 kOe at 100°C. This positive temperature coefficient made MnBi a unique magnetic system that can potentially replace $Nd_2Fe_{14}B$ magnets at higher temperatures. Furthermore, several researchers have made efforts for understanding the mechanism behind the oxidation so that proper optimization can be done to prevent it. One study showed that the perpendicular saturation magnetization of the film can reduce up to 35% after an exposure to the ambient conditions for a period of 4 days. However, capping the film with Ta shows the Hc being increased by 23% after subjecting the film to the same conditions[68].

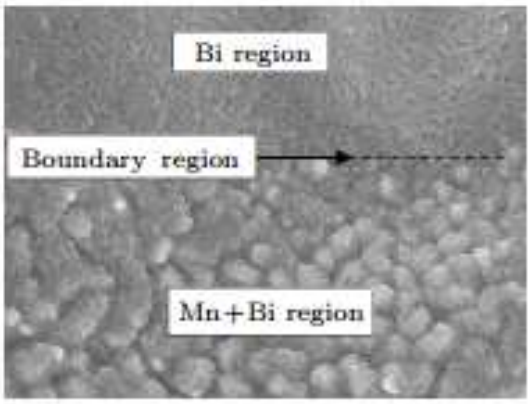

Figure 6. The SEM image of Bi film with and without the top Mn layer annealed at 350 °C for 20 min. Republished with the copyrights from [41].

2.3 MnBi nanoparticles

Analogous to the bulk and thin film, the nanoscopic counterpart of the bi-metallic MnBi magnetic alloy also attracted a lot of attention as a rare-earth-free alternative to the rare-earth magnets. Significant efforts have been made to reach the energy product of the Nd-Fe-B, 59 MGOe, which is the world's largest reported energy density thus far[59, 61]. Research has shown that the energy product of a magnetic material is dependent on its saturation magnetization (Ms) and coercivity (Hc). However, it is a challenge to synthesis a magnetic material that simultaneously exhibits large Ms and Hc, as the former is a property of a soft-magnet whereas, the latter a hard-magnetic property. A promising technique to promote both the above-mentioned properties in a magnetic material is via "exchange coupling", where soft and hard magnetic materials are fused together to give a good interface

between them[69-72]. Research has shown that exchange coupling between magnetically soft and hard materials can give large energy product, given that the parameters are maintained within a certain limit (soft phase no more than double the domain size of the hard phase)[73]. The MnBi has shown large coercivity at the bulk and thin-film structures. Similar, or even better, results can be expected from the nanostructures of the MnBi. Furthermore, a positive temperature coefficient for the coercivity makes MnBi a unique magnetic system and its energy density surpassed the NdFeB magnets at higher temperatures. This makes MnBi a good candidate for the hard-magnetic part of the hard/soft composite for the exchange coupling [74]. Hence, material researchers have attempted several methods to synthesize MnBi nanoparticles in a facile and an environmentally friendly method.

Lam et al., in 2015, successfully demonstrated the fabrication of MnBi nanoparticles by following an extensively explored and well-utilized method that is known as high energy ball milling[74]. To begin, the high-quality ingot was prepared by arc melting Mnand Bi with an atomic ratio of 55:45 (Mn:Bi). It is also important to note that Mn precursor was added at an excess of 15 wt% to compensate the loss of Mn due to the oxidation. The ingot was then crushed into smaller pieces, which were then ball milled into nanoparticles. The size of the particles was largely dependent on the time of milling. Increasing the time of milling from .5 hr to 2 hours reduced to the particle size to about 25 nm. However, there was no noticeable reduction in the particle size for milling time > 4hours. This could be due to the cold welding occurring at the molecular scale that could result in the particles getting larger. Concomitantly, the milling time also affected the magnetic properties of the sample. This could be due to the fact that magnetic properties of a material extensively depend on its grain size. As seen from the XRD results, there is a significant reduction in the grain size of the specimen (~40 nm to ~25 nm) when the milling time increases from .5 hr to 2 hours. However, the grains size grew larger with any further milling. On the other hand, the coercivity of the specimen increased drastically from 7 to 16 kOe when the milling time was increased from .5 hr to 2 hours. There was a smaller increment in the coercivity, from 16 to 17 kOe, when milled for 4 hours. After this, there was a noticeable decrease in the coercivity as the specimen was milled for 8 hours. Though 4 hours of milling gave larger grain and particle size, the largest coercivity at this milling time made it the optimal milling time for highly coercive $Mn_{55}Bi_{45}$. The Ms of the sample shows an opposite trend as it steadily increases with increase in the milling time. This opposite behavior between the Ms and the coercivity is due to the presence of larger volume fraction of the ferromagnetic MnBi when the specimen was milled for longer time. Whereas, the presence of more non-ferromagnetic component, at shorter milling time, isolates the ferromagnetic components, thus increasing the coercivity of the specimen. Contrastingly, annealing the specimen (200 °C and 300 °C) only slightly enhances the magnetic properties and the M_s remained ~50 Am^2/kg. It is crucial to note that milling the MnBi at 1:1 ratio but with the ball to powder weight ratio being 15:1 produced MnBi/Bi particles ~ 100-300 nm with a coercivity of 16.3 T[75]. In this work, the Mn was milled with Bi_2O_3, instead of Bi, in the presence of Ca that played the role of the reducing agent and CaO as the dispersant.

Doping a soft magnetic material in a system of hard magnetic phase had displayed a high saturation magnetization and a high coercivity, however, this technique reduced the Curie temperature of the specimen thus, limiting its practical applications. However, this issue is eliminated by synthesizing magnetic composites that exhibit exchange coupling within themselves. A novel method to fabricate one such composite is via self-assembly of the MnBi nanoparticles and FeCo nanoparticles [76]. MnBi was synthesized via the arc melting of the Mn and Bi precursors before grinding them. The ground powder was annealed followed by ball milling to give a nanoscopic structure. On the contrary, the soft magnetic FeCo nanoparticles were synthesized by a simultaneous reduction of $FeCl_2$ and $CoCl_2$ in the presence of the Oleic Acid. The self-assembly took place in the solvent (hexane) that had FeCo dispersed in it prior to the MnBi addition into the solvent. The MnBi was added into the hexane/FeCo solution, leaving the FeCo on the MnBi as the soft magnetic particles were attracted by the hard magnetic MnBi. The grinding also reduced the MnBi grain size for high coercivity, as the size of the grains were enlarged after the annealing process. After the final grinding, the MnBi grain size was close to its single domain size that resulted in a high coercivity (8.2 kOe). Whereas, the FeCo particles were as small as 5-10 nm. Studying the two different samples for their magnetic properties, it was found that the sample with only 10wt% of FeCo displayed slightly higher Ms than that of the sample with 5wt% of FeCo (Figure 7). However, the drop in coercivity with an increase in the soft magnetic phase makes the sample with only 5wt% the better choice. This conclusion is also backed by the Henkel plot (Figure 8) that shows a large positive ΔM, indicating exchange coupling between MnBi and FeCo phases. A Henkel plot is a specific relationship between M_r, M_d and M_{inf} that are required to determine magnetic interaction in permanent magnets, soft magnets, superconductors, data recording and magnetism in rocks. Interpretation of the plot is a key tool in magnetic research as it illuminates the valuable details about the interaction mechanism that governs the magnetization of a magnetic material [77].

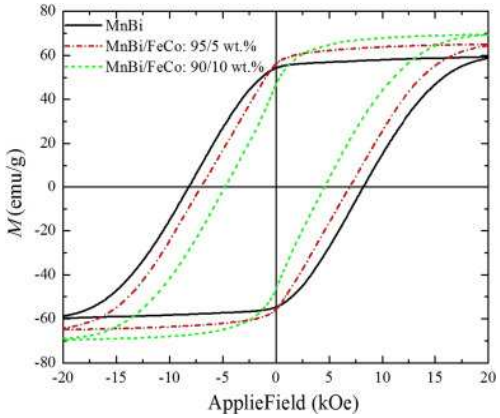

Figure 7. Magnetic hysteresis loops of the MnBi particles and MnBi/Fe-Co (95/5wt% and 90/10wt%) after 5 min grinding. Republished with the copyrights from [77].

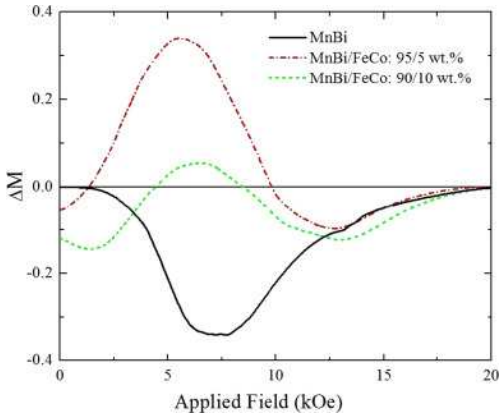

Figure 8. The ΔM curves of MnBi and MnBi/FeCo (95/5wt% and 90/10wt%). Republished with the copyrights from [77].

3. Structure and magnetic properties of MnAl magnetic materials

Currently, the Nd-Fe-B and Sm-Co are being extensively being utilized given that they possess incredibly large energy densities 56 MGOe and 30 MGOe, respectively[78, 79]. However, the high cost and the depletion of the rare-earth metals in near future has forced researchers and scientists to invest their efforts towards finding a replacement for the above-mentioned magnets. Low cost, due to the abundance in the earth's crust, moderate energy density and the large magnetic anisotropy (107 erg/cc) has encouraged material scientists to couple Mn and Al together for a variety of applications such as magnetic recording, perpendicular magnetic anisotropic material and data storage[27, 80, 81]. Appreciable amount of research, since 1958, has shown that the large anisotropy is observed in the metastable $L1_0$ phase, also known as the τ-MnAl. The τ-phase can only be achieved by cooling hexagonal ε-phase[27, 82, 83]. Therefore, synthesizing MnAl complex with a large τ-phase content is accompanied by a strenuous challenge. Research has also shown the Ms of the material to reach to 490 emu/cc for thin films and 89 emu/g for its bulk counterpart. Furthermore, the structure of MnAl alloy resembles that of the FePt that can be reduced to the tetragonally distorted B2 structure, resulting in higher anisotropic output[84-86]. In the crystal, Mn resides at the corner sites while Al occupies the center location making the entire crystal to be like Mn and Al existing with alternating planes along the tetragonal c-axis. Another challenge in the fabrication of τ-MnAl is the small stoichiometric window as both the elements need to be at ~1:1 atomic ratio. Therefore, a high chemical order is essential. Furthermore, in case of the thin-films, the film is sensitive to the templating strain during the crystallization, which demands the selection of appropriate substrate to grow the film[87-90]. Majority of the work reported was attempting to exploit the magnetic complex for the perpendicular anisotropy applications, therefore, the thin-film structure. Only a few studies have been reported on the magnetic bulk and nanoparticle synthesis of the MnAl system.

3.1 MnAl bulk materials

High-quality bulk permanent magnets are crucial components of efficient motors utilized to generate power from the wind turbines and in the electric/hybrid cars. Apart from the final output of the generated power, the quality of the magnets also dictates the size of the motors. Hence, permanent magnets with large energy product are always in demand. Many reports have indicated towards MnAl being a reliable replacement for the expensive rare-earth metal magnets thus, attracting more attention. Also, among all the phases of MnAl, it is the τ-MnAl that possesses ferromagnetic characteristics. Therefore, various synthesis techniques have been and are still being experimented with to synthesize the τ-phase MnAl and to reach the theoretical energy density of the MnAl system.

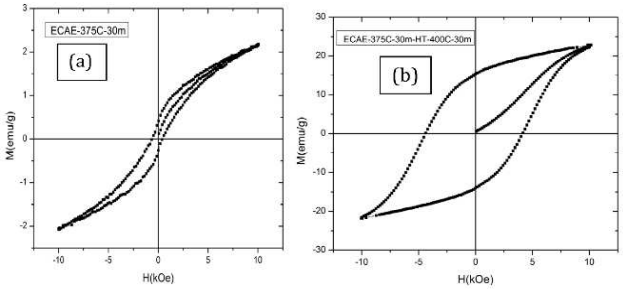

Figure 9. Magnetic hysteresis measurements from (a) a billet extruded at 375 °C, and (b) the same billet after thermal treatment at 400 °C for 30 min. The specimen was prepared from mechanically-milled gas atomized powder. Republished with the copyrights from [91].

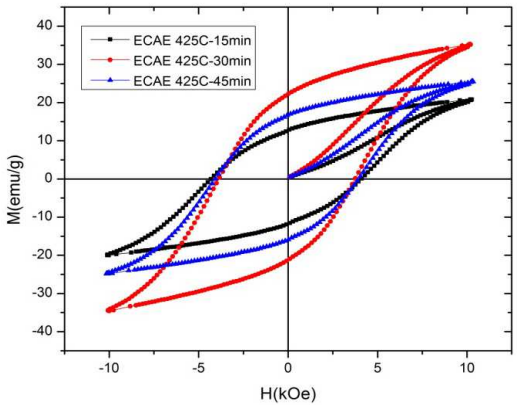

Figure 10. Magnetic properties of three billets extruded from gas-atomized particles milled for 20 h within a large attritor extruded at 425 °C for the time of 15, 30 and 45 min. Republished with the copyrights from [91].

Hot extrusion method is a commonly opted technique by the material scientists and chemists for synthesizing alloys and it has also been utilized to form τ-MnAl. However, the challenge to create a MnAl system with 100% τ-phase is still unsolved. Chaturvedi et al. reported the fabrication of τ-MnAl via equal channel angular extrusion (ECAE), also known as equal channel angular presser (ECAP)[91]. Producing high-quality ε-phase and then transforming it into the τ-phase has been the key to obtaining the high magnetic anisotropy thus far. A study conducted to interpret the structure of the defects and the nature of the phase transformation to understand the construction of the ferromagnetic τ-phase showed that the ferromagnetic behavior in the MnAl system is exhibited due to the ε to τ phase transformation. During the transformation, many defects are generated that promote the high magnetic

anisotropy. Furthermore, during the phase transformation, small percentage of stable phases like γ2 and β get trapped at the magnetic domain boundaries, which results in a significant increase in the coercivity. In the study conducted by Chaturvedi et al., the test specimen was prepared via gas atomization of Mn-46 at.% Al powders under gas Ar gas protection. Mechanically milling the samples generated the nanocrystallites of the ε-phase. Analyzing the as-received powder by XRD shows ~66% of ε-phase and rest being a mixture of γ2 and β-phases. However, after the ECAE, a mechanical milling for 20 hours spawned ~61% of the metastable τ-phase (Figure 9). The magnetic measurements revealed a negligible signal for 375 °C extruded sample but the 400 °C extruded sample turned out to be ferromagnetic with a coercivity of 4.4 kOe and Ms around 23.2 emu/g. The values are lower than that of reported by Zeng et al. and this could be resulted from the sample consisting of 100% ε-phase, whereas Chaturvedi's sample only consisted around 66% ε-phase [92]. Furthermore, the magnetic properties were enhanced by increasing the extrusion temperature to 425 °C for 30 mins (Figure 10). The sample was also stable in air at 200 °C for around 40 days. This demonstrated the longevity of the metastable phase of the MnAl. In general, the stability in MnAl can be generated via doping C element, however, some research has also shown doping Ni and Co can also increase the stability of the τ-MnAl. It has been reported that the hot extruded method can be used to study the process of magnetization reversal in the τ-MnAl-C. As previously mentioned, the C doping here stabilizes the tetragonal phase. Kerr microscopy was utilized to reveal the magnetization reversal (Figure 11)[93]. It also revealed that the microstructure consisted of large non-recrystallized and fine recrystallized grains. The studies confirmed that a fully recrystallized microstructure is essential for obtaining high coercivity.

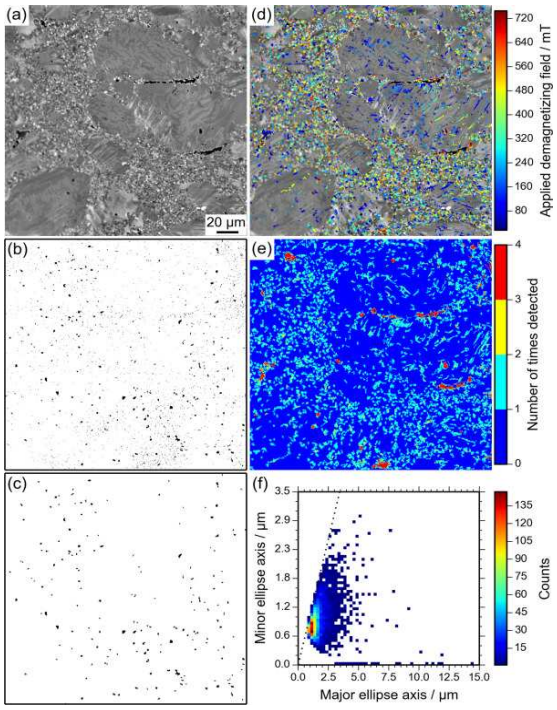

Figure 11. The Kerr image analysis. (a) Kerr image in zero-field after magnetizing the sample with a magnetic field pulse of 3 T. (b) The difference image of the Kerr images taken at the demagnetizing fields of 338 mT and 357 mT. (c) Size filtered image resulting from the image in (b). (d) The same image as in (a) overlaid with the switched regions detected at all applied field directions. The color code shows the applied field at which the switch was detected. (e) The image formed by summing the difference images from the entire series after applying the size filter. The color scale shows how many times each pixel was detected. (f) The 2D histogram showing the lengths of the major and minor axes of ellipses fitted to the detected regions. The dotted line shows a ratio of the major to minor axis of 1. Republished with the copyrights from [90].

3.2 MnAl thin film

The MnAl thin-film structure is majorly utilized for the magnetic tunneling junction applications, such as ultrahigh-density spin transfer switching random access memory (Spin-RAM), magnetic random-access memory (MRAM), and spin-logic circuits due to its appreciably high perpendicular magnetic anisotropy. Theoretical analysis has shown that the saturation magnetization and Gilbert's constant (α) are directly proportional to the switching current density (J_{co}). Therefore, the ferromagnetic materials with low M_s, α and large anisotropy energy (K_u) are the ideal material choice to achieve a high recording density with a minimum power consumption for Spin-RAM[94, 95]. The above-mentioned properties together with the low fabrication cost encourage the researchers to investigate the MnAl thin films.

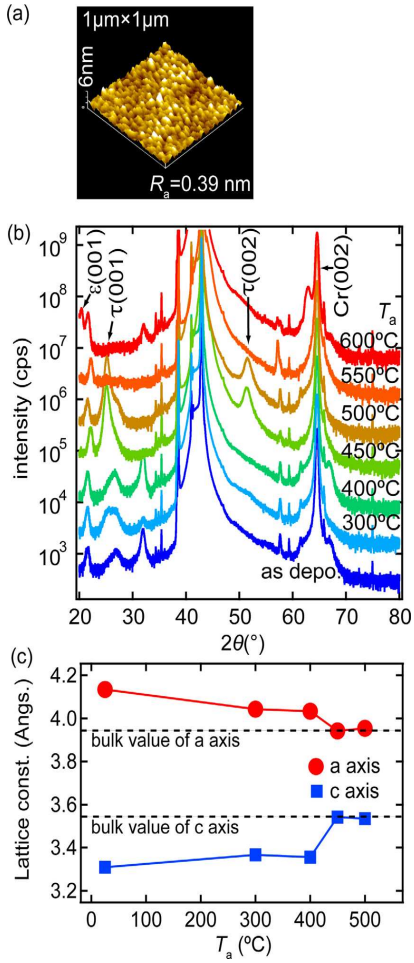

Figure 12. a) The AFM image of $Mn_{48}Al_{52}$ thin film with $T_{s\text{-}}$200 °C and T_a450 °C. (b) Annealing temperature (Ta)-dependent XRD patterns. (c) Ta-dependent lattice constant for $Mn_{48}Al_{52}$ thin film with $T_{s\text{-}}$200 °C. Republished with the copyrights from [95].

Hosoda et al. reported the fabrication of $L1_0$-MnAl thin films that were perpendicularly magnetized for magnetic tunneling junction applications[95]. In their work, they selected single crystal MgO (001) as the substrate to grow the film to reduce the lattice mismatch between the film and the substrate. The lattice mismatch may develop strain between the layers of the film if it grows onto the mismatched substrate. This can be detrimental for achieving the easy axis in the 'c' direction. Furthermore, a Cr buffer layer was also made for further enhancing the film growth. The films were prepared by a magnetron sputtering system, at 10-7 Pa base pressure, in the order of substrate/Cr (40nm)/MnAl (50nm)/Ta. Tantalum serves as a capping layer to protect the film from oxidation. To elucidate the stoichiometry dependent magnetic properties, three different samples were prepared: $Mn_{46}Al_{54}$, $Mn_{48}Al_{52}$, and $Mn_{50}Al_{50}$. Fabricating these films at T_s = 200 °C and annealing them at various temperature (T_a), followed by analyzing them under XRD revealed that τ-MnAl peaks were clearly observed for T_a = 450 °C and 500 °C (Figure 12). However, the peaks started to diminish as Ta increased to 550 °C and 600 °C. This showed that the T_a for the thin film is like that of their bulk counterpart. Furthermore, $Mn_{48}Al_{52}$showed the highest peak intensity thus leading to the selection of $Mn_{48}Al_{52}$ for further investigation. Ta dependent magnetic analysis showed the highest values of M_s and K_u (600 emu/cm^3 and 107 erg/cm^3 respectively) for T_a = 450 °C. Also, it was evident that the magnetic properties declined with further increase in temperature. It is also noteworthy that the substrate heating temperature (the fabrication temperature) T_s also played an important role in bringing out the magnetic characteristics of the MnAl system. It was found that 200 °C is the appropriate T_s as the samples prepared at T_s = 300 °C exhibited lower M_s and K_u than the samples at T_s = 200 °C. Furthermore, the samples prepared at room temperature did not show any perpendicular magnetic characteristics regardless of the T_a. This study revealed two important factors, including the dependence of the perpendicular anisotropy on annealing temperature and the substrate temperature. Furthermore, the study also revealed the appropriate stoichiometry of Mn and Al for the essential for the ferromagnetic nature.

The right selection of a substrate is an integral step towards growing high quality thin-film magnetic material. Because, with similar lattice structure as that of the film significantly reduces the lattice strain, which concomitantly promotes better film growth with high perpendicular anisotropy. This led Cui et al. to study the thickness dependent anisotropy in an epitaxially grown τ-MnAl thin films[94], using the "biased target beam deposition system" (BTBDS) to form quasi-monolayer deposition. This enhances the crystallinity of the MnAl thin film and promotes better τ-phase formation. It was noteworthy that ferromagnetic thin films were only possible for the deposition at room temperature. The stoichiometric conditions for the formation of τ-phase requires Mn to be in the range of 50-60 atomic percentage. This criterion was fulfilled during the fabrication via BTBDS, as shown by the compositional analysis. Furthermore, analysing the film by XRD after annealing the as-prepared film at 400 °C for 12 s revealed the formation of τ-phase. Comparing the XRD spectra of before and after annealing the samples elucidates that annealing is crucial for the formation of the τ-phase (Figure 13). It was found that due to the coherent interface, there was a lattice mismatch of ~6.7% that caused a large tensile strain in the 10-nm thick film. In addition, a reduction in the 'c' lattice was observed (3.57 Å to 3 Å) that was a result of the in-plane tensile strain as described by the Poisson's effect. These results suggest an epitaxial growth of the τ-MnAl film on the MgO substrate. Furthermore, Bethe-Slater curve reveals the positive exchange coupling between the 3delectrons of the adjacent Mn atoms. This gives rise to a saturation magnetization of 394 emu/cc, which is lower than that of bulk data ~490 emu/cc. Subtracting the dead layer gives the value ~523 emu/cc (~1.9 μB/Mn), which is very close to the theoretical prediction (~1.975 μB/Mn). It is suggested that the lower value of Ms could be attributed to the defects in the film such as antiphase boundaries and/or due to a dead layer at the interface between the Ta capping layer and the MnAl thin film. Additionally, the magnetic analysis showed that the bi-layer thickness ~5.7nm turns out to be the optimum. Thinner films tend to disrupt the atomic composition that lead to less ferromagnetic material whereas, thicker films generated additional non-magnetic phases such as γ2-MnAl and β-MnAl that resulted in a lower magnetization. In addition, repeating the optimized bi-layer enhanced the anisotropy (Ku) and at 10 times of repetition, the optimum Ku was obtained (1.2 x 106 erg/cc). Further increasing the repetition to 18 times showed a negative Ku (-0.7 x 10^5 erg/cc), which could be due the dominance of the in-plane anisotropy. Besides, using MgO as the substrate and Ta as the capping layer, Saruyama et al., introduced Cr as a buffer layer between the MgO and MnAl, which appears to further reduce the lattice mismatch and enhanced the magnetic properties of the MnAl[96]. This makes MnAl more applicable for magnetic tunneling applications. Also, it is to note that the films were prepared by intentionally heating the substrate at Ts = 250 °C. As discussed before, the intentional heating of the substrate can promote the formation of the ferromagnetic τ-phase. Figure 14clearly shows the enhanced magnetization. In addition, the difference in the perpendicular and parallel magnetization suggested that the material needed more than 20 kOe of external magnetic field to fully saturate them. This demonstrates the feasibility of the specimen to be applicable for magnetic tunneling applications. Another technique for boosting the magnetic properties of a material was investigated by Fischer and Rudee[97]. The MnAl had a small percentage of Ni and C that make final composition of the magnet as $Mn_{68.8}Al_{29.98}Ni_{0.78}C_{0.44}$. Research has shown that for MnAl to consist of τ-phase, Mn has to be in the range of 50-60 wt%. Exhibiting ferromagnetic characteristics even when being out of the range may be attributed to the presence of Ni and C. Fischer and Rudee reported that annealing MnAl in the presence of an external magnetic field can cause a notable improvement in the magnetic properties of MnAl[97]. This technique can possibly be translated into regimes of other magnetic materials as well. The samples were cut into two pieces and annealed with and without the presence of an external magnetic field (15kOe), respectively, keeping the annealing temperature constant at 410 °C in both cases (Figure 15).

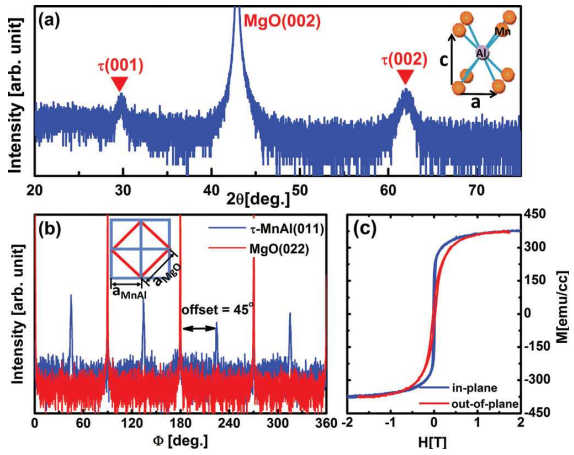

Figure 13. (a) The 2θ scan of MnAl thin films $[(Al/Mn)(5.7\ Å)]_{18}$ on MgO(001). The inset of (a) shows the structure of τ-MnAl unit cell. (b) The ϕ scans on the $[(Al/Mn)(5.7\ Å)]_{18}$ sample. The blue line represents data taken at 2θ of 42.37° (τ-MnAl (011) peak) and the red represents the result taken at 62.45° (MgO (022) peak). The inset of (b) shows the matching strategy between MgO and τ-MnAl lattice. (c) In-plane (blue) and out-of-plane (red) magnetic hysteresis loops of $[(Al/Mn)(5.7\ Å)]_{18}$ sample. Republished with the copyrights from [94].

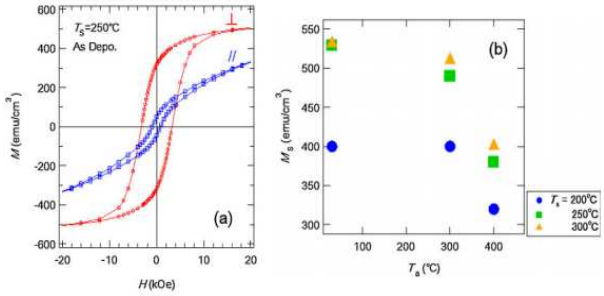

Figure 14. (a) Magnetization hysteresis curves for the Cr/MnAl/Ta thin films prepared at $T_{s\text{-}¼}$ 250 °C. (b) Annealing temperature (Ta)-dependent saturation magnetization for Cr/MnAl/Ta films prepared at $T_{s\text{-}¼}$ 200, 250, and 300 °C. Republished with the copyrights from [96].

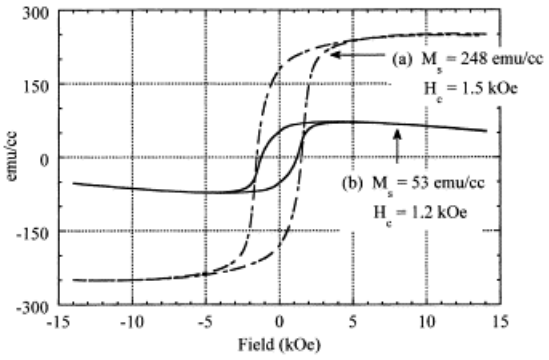

Figure 15. Comparison of the zero-field annealed 2000 Ångström sample (a) to the sample with the thickness of 2000 Ångström annealed in a 15 kOe field, (b); both sample were annealed at 410 °C. Republished with the copyrights from [97].

3.3 MnAl nanoparticles

The MnAl nanoparticles have not been studied as much as its thin-film and bulk counterparts. At the nanometer scale, materials usually exhibit quantum mechanical characteristics and properties that are not observed at their bulk scale. The uniqueness of these quantum mechanical properties has led scientists and researcher to investigate the nanoscale regime of numerous materials[98-105]. For MnAl, it is possible to fabricate the material at its single domain size, the result of which has been reported to bring out the maximum coercivity of the magnetic material. Fabricating near single-domain sized MnAl nanoparticles can possibly enhance the energy product of the material, taking it one step closer to replacing the rare-earth magnets. However, there is a significant lack of research that is needed to be done.

One of the methods of fabricating the MnAl nanoparticles is via ball milling the bulk MnAl. Su et al., in 2016, used the same technique and brought the bulk ε-MnAl down to nanometer scale in the presence of surfactants[106]. They were successful in reaching 60-90 nm size range of the MnAl flakes, which also showed the change in particle sizes dictated by the oleic acid and oleyl amine. The surfactants assist in controlling the size of the particles and reduce the chances of the cold-welding. There was no observable transformation in the phase in the as-milled (12 hr long) MnAl flakes, which also indicated no change in the stoichiometry ($Mn_{54}Al_{46}$), showing their immense stability. However, annealing the bulk ingot sample at 500 °C for 30 min caused the ε-phase to transform into τ-phase with a small percentage of the non-magnetic γ2 and β-phases. By following a time-dependent surfactant assistant milling, Su et a. were successful in fabricating the ferromagnetic τ-MnAl (Figure 16). Apart from the ligand-assisted ball milling, Shen et al., reported a ligand metal-redox method to synthesize MnAl nanomagnetic particles[107]. The synthesis took place in a standard Schlenk line system, where the reduction of the precursors takes place by the difference in their respective potentials ($Mn_2(CO)_{10}$, E0 = -1.19 V, $AlCl_3$, E_0 = -1.66 V). Furthermore, LiAlH4 was added to assist the reduction of aluminum chloride. The study involved the optimization of the reaction temperature and reaction time along with doping transition metals into the MnAl system. Among Ni, Co and Fe only Co doped sample showed a notable magnetism. In addition, it was found that the interplanar distance of the Co doped samples matched with that of $MnAlCo_2$, suggesting the formation of the ternary nanocrystals. Furthermore, stoichiometry dependent study revealed that $Mn_{90.8}Al_{0.1}Co_{9.1}$ exhibits the highest M_s and coercivity. Any further increase in the Co content resulted in a drastic reduction in the coercivity.

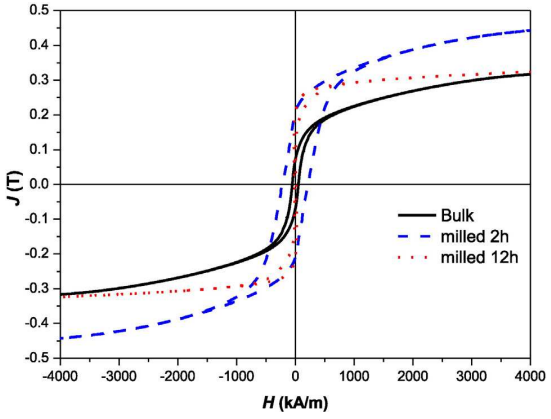

Figure 16. Magnetic hysteresis loops for bulk and $Mn_{54}Al_{46}$ flakes. Republished with the copyrights from [106].

4. Structure and magnetic properties of MnGa magnetic materials

Since the last two decades, MnGa has received a lot of attention as a favourable material of choice for spintronic devices, permanent magnets and magnetic recording applications [108-112]. Theoretical calculations have shown that MnGa with $D0_{22}$ (ferrimagnetic) and $L1_0$ (ferromagnetic) crystal structure can exhibit large perpendicular anisotropy. The theoretical calculations have demonstrated, for $L1_0/D0_{22}$-MnGa, M_s ~845/305 emu/cc, K_u ~26/20 Merg/cc, (BH)max ~ 28 MGOe[23]. These exciting numbers are very much suitable for their technical applications and thus, have encouraged researchers to put their effort into reaching the theoretical values hence, resulting in a numerous reported work. Furthermore, should the above mentioned theoretical values are obtained, the increasing demand for cheaper and more efficient magnetic material with high perpendicular magnetic anisotropy can possibly be met.

4.1 MnGa thin films

Majority of the work reported on MnGa has featured MnGa with a thin film structure, as attempts to obtain its theoretically predicted magnetic properties[111-119]. For example, Zhao et al., reported a study on the magnetic and structural properties of Mn-Ga thin films to recognize the mechanism of its magnetic anisotropic[120]. In their work, several samples of the form [MnGa 2-nm/Mn x-nm] were prepared via DC magnetron sputtering on Si substrate. The samples consisted of $Mn_{56}Ga_{44}$, $Mn_{59}Ga_{41}$, $Mn_{61}Ga_{39}$, $Mn_{63}Ga_{37}$, $Mn_{68}Ga_{32}$, $Mn_{71}Ga_{29}$, $Mn_{76}Ga_{24}$, $Mn_{79}Ga_{21}$, $Mn_{82}Ga_{18}$, $Mn_{84}Ga_{16}$, $Mn_{86}Ga_{14}$, and x ranging from .2 to 3.5. In addition, the samples were annealed at a range of 300 ˚C to 400 ˚C for about 10 hours. The magnetic measurements were conducted from -270 °C to 127 °C. Analyzing the as-prepared samples under XRD showed only slight peaks of $D0_{22}$-phase. This was an indication of the sample of being amorphous or nanocrystalline. The transmission electron microscopy (TEM) images later clarified the ambiguity as it showed nanocrystalline materials that matched with the XRD data, suggesting the presence of the $D0_{22}$ phase (Figure 17). The in-plane and out-of-plane M-H loops showed that the magnetic properties were significantly altered with a change in the value of x (Figure 18). Furthermore, the group studied the correlation between Ku and Ms of the magnetic sample following the methods that has been used in the past for similar studies. Studying the correlation between the Ku and Ms of samples with x = 0.5 and 2.5 at -270 °C showed that Ku for both the samples followed the nth power of dependence of their respects Ms.

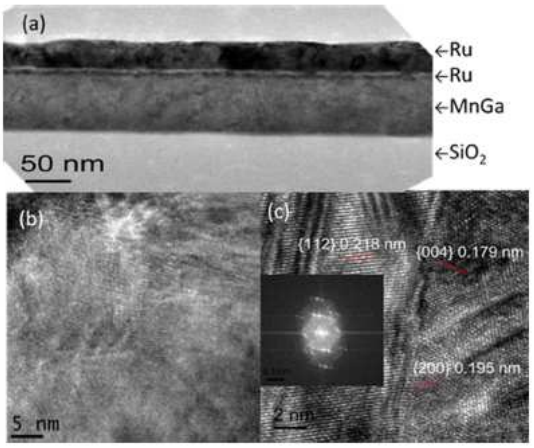

Figure 17. (a), (b) The low magnification and (c) high magnification cross-sectional TEM images for the sample with x = 2.0. The inset figure of (c) shows the fast Fourier transformation of the image (c).Republished with the copyrights from [120].

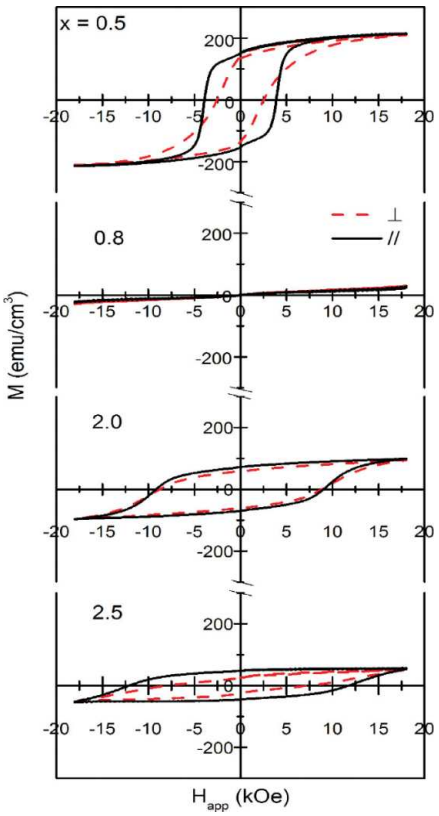

Figure 18. The magnetization hysteresis curves measured for the samples with the various Mn layer thicknesses x and Ta = 325 ^{0}C in the applied fields of 18 kOe. Republished with the copyrights from [120].

We have discussed the importance of the selection of the appropriate substrate for the film growth. Especially for the magnetic materials, the intrinsic magnetic properties largely depend on their crystal and lattice structure, which includes the shape and the size of the particles. In addition to that, the lattice mismatch between the substrate and the film grown on to the substrate is an important driving force towards obtaining large perpendicular anisotropy. Therefore, it is

crucial to understand how MnGa thin-films are affected by the substrates. Substrates like GaAs, MgO and Si have been extensively exploited to grow MnGa. Feng et al., conducted a similar study where they utilized two different substrates, Si/SiO_2 and glass, to understand the growth of MnGa on the chosen substrates and their coercivity mechanism[110]. In their study, they used DC magnetron sputtering to grew the thin-films with various thickness ranging from 10-50 nm using a DC magnetron sputtering in a high vacuum chamber. There were also under-layers (Mo, Pd, MgO and Ta) fabricated on the three different types of substrates. There prepared films had the following structures: i. Si/SiO2 substrate/$MnGa_x$/Ta(10 nm); ii. glass substrate/ $MnGa_x$ /Ta(10 nm); and iii. Si(100) substrate/underlayer(10 nm)/ $MnGa_x$ /Ta(10 nm); (x = 10–50 nm).

They used two different target sources T1 ($Mg_{70}Ga_{30}$) and T2 ($Mg_{60}Ga_{40}$). The 10 nm of Tantalum layer was used as a protective layer. When sputtered on the substrate heated at 200 °C, the sample gave an amorphous signal when analyzed under X-ray. However, for the samples (from T1 and T2) grown on the substrate temperature 450 °C, both the tetragonal $D0_{22}$ and $L1_0$-phases were observed. Based on the PDF of $D0_{22}$ and $L1_0$-MnGa, the films grown on SiO_2 tend to be magnetically isotropy. However, numerous research has shown that isotropic MnGa thin films can be better than the anisotropic films with a coercivity of 20.5 kOe at room temperature for $Mn_{67}Ga_{33}$ grown on SiO_2. Analyzing the in-plane and out-plane M-H loops for the samples shows a clear difference in the magnetic properties with respect to the choice of the substrate (Figure 19). Furthermore, the linear relationship between the magnetization and the applied field suggest that the coercivity follows the nucleation-controlled mechanism. In addition, the in-plane and out-of-plane data are much better for the films grown on SiO_2 than those of grown on Si substrate. Furthermore, Mo and Pd under-layers further enhanced the coercivity of the thin films. The improvement can possibly be due to the better crystallinity and improved texture of the films. Also, the substrate temperature, Ts, effects the final magnetic properties. Increasing the Ts showed a notable rise in the coercivity of the MnGa thin films with the maximum value at T_s = 450 °C. For T_s= 300 °C, both the Ms and Hc are very small, which could be due to the poor crystallinity of the $D0_{22}$-phase. Additionally, the thickness of the film dictates the magnetic reversal behaviour. Therefore, the coercivity of the thin-films are very small so the reversal is much easier. This not the case as the thickness of the film increases. The increment in the film thickness is directly proportional to the increase in the coercivity, which could be due to the defects in the films. Furthermore, the isolated grains can also play a role in the increased coercivity of the material. Another research has also shed some light on the dependence of the magnetic properties of the MnGa thin-film on the texture of the film. Kazuya et al., prepared ultra-thin films of MnGa to study the effect of the textures on the magnetic properties using the dc magnetron sputtering [112]. It is interesting to note that the films were grown on the SiO_2/Si substrate as demonstrated in the work discussed above. However, various buffer layers and capping layers were implemented in this work (Figure 20). Looking at Figure 21, it is evident that changing the thickness of the highly textured MnGa ultra-thin films largely affect their intrinsic magnetic properties.

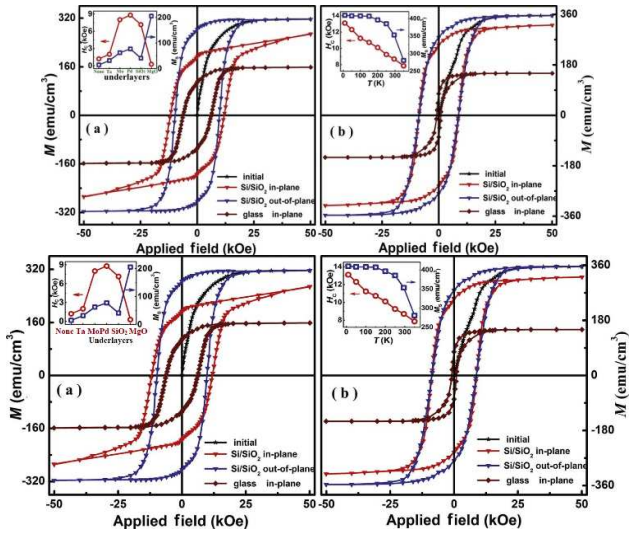

Figure 19. Magnetic hysteresis loops of 30 nm MnGa films sputtered from (a) T1 and (b) T2 at TS of 450 °C. Inset of (a): Dependences of H_C and M_S with different under-layers. Inset of (b): Dependences of H_C and M_S on the measuring temperature. Republished with the copyrights from [110].

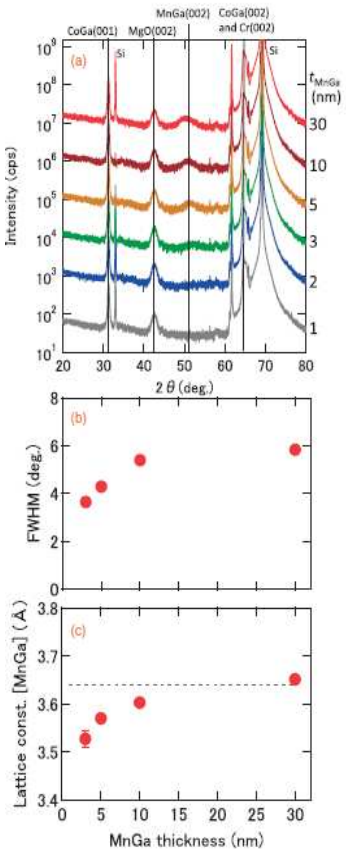

Figure 20. (a) Out-of-plane 2θ–ω scan of the XRD pattern of MnGa layer samples with different thickness. Data are plotted with an offset for clarity. MnGa layer thickness dependence of (b) FWHM of the rocking curves (ω scan) of the MnGa (002) diffraction

peak and (c) the estimated c lattice constant of the MnGa layer. The dashed line denotes the bulk value. Republished with the copyrights from [112].

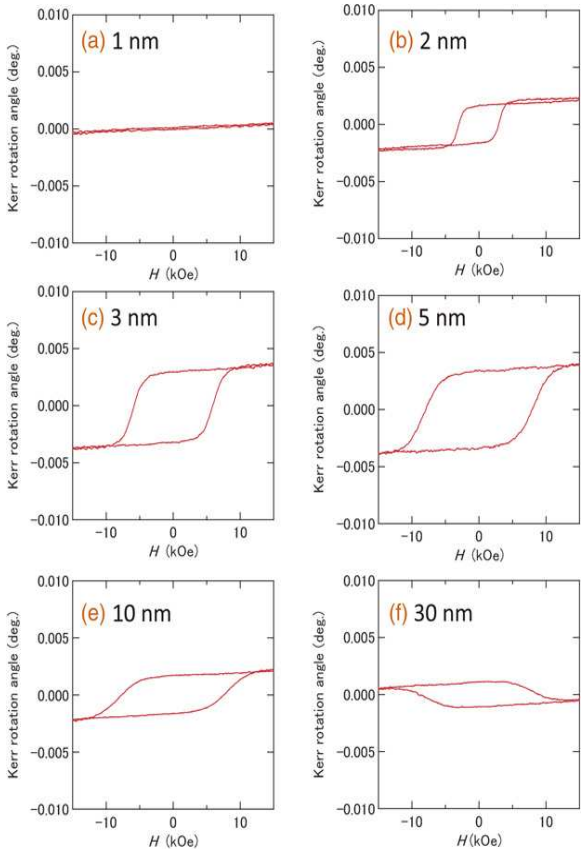

Figure 21. Magnetic hysteresis loops for the magneto-optic Kerr effect (MOKE) of MnGa samples with the layer thicknesses of (a) 1, (b) 2, (c) 3, (d) 5, (e) 10, and (f) 30 nm. Republished with the copyrights from [112].

4.2 MnGa nanoparticles

Magnetic materials have been known to exhibit their maximum intrinsic magnetism when they are at the single domain size. However, there has been only a few reports on the nanoparticles of the MnGa or MnGa based magnetic nanoparticles. Furthermore, Mn-based alloys being one of the most highly attractive material for the replacement of the rare-earth consisting magnetic materials, it makes it more essential to have more research to be done in towards exploring the nanoscale regime of MnGa as well. Few years ago, a study was conducted by Jamer et al., on Mn_xGa to elucidate its magnetic properties and large coercivity[121]. The material was prepared by vapor-liquid-solid (VLS) growth method and followed by the sequential deposition of Mn and Ga by molecular beam epitaxy (MBE). The VLS has been known for the fabrication of nanowires; however, in this work, it was used for the pre-depositing 0.5 nm thick Au layer on silica substrate that led to a uniform nanoparticle growth instead of the nanowire structures. The MBE was then utilized to sequentially deposit Mn and Ga that forms the Mn_xGa nanocomplex (Figure 22). Based on the value of "x" Mn_xGa can exist in several different phases. For $x < 1.6$, Mn_xGa prefers $L1_0$ structure, for $1.6<x<3$, Mn_xGa can have hcp structure that is also antiferromagnetic and for samples annealed at temperature over 600 °C, Mn_xGa can exist in a cubic compensated $D0_3$ phase that is ferrimagnetic. For the samples annealed at lower temperatures, a tetragonal metastable $D0_{22}$ phases existed for Mn_xGa. The sample was annealed at 400 °C after the deposition of Mn and Ga layers. The XRD data matched with the above discussion $D0_{22}$, Bragg's peaks had the highest intensity. Furthermore, it is the $D0_{22}$ component of the sample is the source of the high coercivity. According to the Stoner-Wohlfarth model, the theoretical coercivity of the $Mn_{2.5}Ga$ is calculated to be about 100 kOe. However, the measured coercivity is only 10kOe at 29 °C. The lower value could be due to the lack of the single domain size and due to the presence of some unwanted phases such as $D0_3$ and $D0_{19}$.

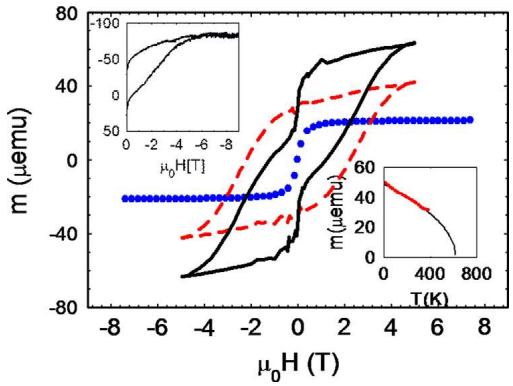

Figure 22. Magnetic moment (solid black curve) as a function of magnetic field for the nanostructured Mn_xGa grown using the Au catalyst and the sequential Ga and Mn deposition. The dashed (red) and dotted (blue) curves are high- and low-coercivity components, respectively. Inset (upper) shows m(H) to 9 T. Inset (lower) shows the low-field (0.1T) moment versus temperature, where the extrapolation gives Tc 327 ˚C. Republished with the copyrights from [121].

MnGa nanoparticles can also be synthesized via the solution approach. This method requires Standard Schlenk line setup, and the entire reaction is carried in an inert environment. Furthermore, surfactants and ligands are essential in this reaction as they control the size growth of the particles. The reaction takes place at ~320 °C for about 120 min. The final obtained product is ferromagnetic in nature with majority of the composition being Mn_3Ga (Figure 23). The reduced coercivity could be due to the composition not being $Mn_{2.5}Ga$ and also due to size of the particles being much smaller than that of their single domain. Further improvements, such as better and more accurate temperature control, are required in this technique to control the size to a near-single domain range. In addition, the stoichiometry needs to be optimized as well. If done so, this technique can be an easy and a low-cost method for the MnGa nanoparticle synthesis.

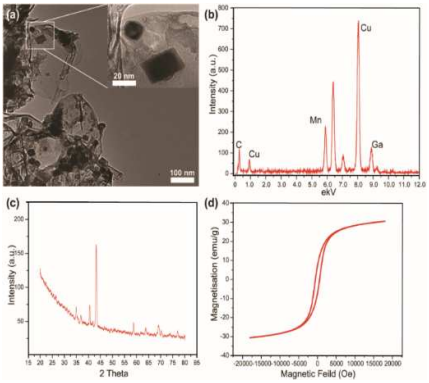

Figure 23. (a) TEM image, (b) EDS mapping, (c) XRD spectrum and (d) M-H loop of the MnGa nanoparticles synthesized via colloidal solution approach.

Conclusion and prospects

The rising demands for more efficient, cheaper, and more environmental-friendly magnetic materials are the requirement for a safer and greener future in magnetic material manufacturing. The strategic location of the rare-earth metals has increased their price based on the increased toxicological evaluation level on the environment and workers. The Mn element, being highly magnetically active and abundant in our earth's crust, drew a lot of attention. Furthermore, theoretical simulations and calculations have shown exciting data for the Mn-based magnetic alloys. Hence, many studies have been conducted on Mn-based nanomagnetic alloys, namely MnBi, MnAl and MnGa to elucidate the mechanism of the magnetic anisotropy in them and to reach the theoretically predicted magnetic properties. Despite the amount of work reported in this regime, there is still a lot of areas to explore. For example, a significant amount of work is required for the growth of high-quality nanoparticles. This may be achieved by proper selection and optimization of the synthetic procedure. For example, using the standard Schlenk line has shown a control for nanoparticle growth. However, maintaining the appropriate heating rate is a key during the process. Also, the increasing energy density of MnBi has shown the possibility of being able to reach its theoretically predicted energy density. The same is applied for the case of MnBi-thin films and nanoparticles. Exploring the lattice-matched suitable substrates for bottom-up growth of the thin-films can largely assist towards enhancing the magnetic anisotropy. With constant efforts being made, we may expect to see some further exciting results for MnBi in the coming decade or two. On the other hand, MnAl and MnGa need some more attention as most of the work done featuring MnAl or MnGa appears to be in their early stages. With the aid of molecular simulations, we can facilitate the understanding of the origin of the enhanced magnetocrystalline anisotropy in Mn-alloy magnetic nanostructures. Furthermore, the RE- free magnetic materials can also be used in conjunction with the RE magnetic material, hence minimizing the use of the RE magnetic materials. In conclusion, the reported work, featuring Mn-based magnetic alloys (MnBi, MnAl, MnGa), have shown the potential to be the alternatives for the replacement of the rare-earth magnetic materials. However, a lot of work and effort is still required before the above-mentioned alloys can be used as the replacements.

Conflicts of interest

There are no conflicts to declare.

Acknowledgements

S.R. thanks the financial support from the U.S. National Science Foundation (NSF) under the CAREER Award No: NSF-DMR-1830749.

Notes and references

1. Bailey, G., N. Mancheri, and K. Van Acker, *Sustainability of Permanent Rare Earth Magnet Motors in (H)EV Industry.* Journal of Sustainable Metallurgy, 2017. **3**(3): p. 611-626.
2. Faiz, J., H. Nejadi-Koti, and Z. Valipour, *Comprehensive review on inter-turn fault indexes in permanent magnet motors.* Iet Electric Power Applications, 2017. **11**(1): p. 142-156.
3. Sreenivasulu, K.V. and V. Srikanth, *Fascinating Magnetic Energy Storage Nanomaterials: A Brief Review.* Recent Patents on Nanotechnology, 2017. **11**(2): p. 116-122.
4. Yue, M., X.Y. Zhang, and J.P. Liu, *Fabrication of bulk nanostructured permanent magnets with high energy density: challenges and approaches.* Nanoscale, 2017. **9**(11): p. 3674-3697.
5. Kotschau, A., et al., *Sunflower (Helianthus annuus): phytoextraction capacity for heavy metals on a mining-influenced area in Thuringia, Germany.* Environmental Earth Sciences, 2014. **72**(6): p. 2023-2031.
6. Liang, T., K.X. Li, and L.Q. Wang, *State of rare earth elements in different environmental components in mining areas of China.* Environmental Monitoring and Assessment, 2014. **186**(3): p. 1499-1513.
7. Miller, J.R., *Forensic Assessment of Metal Contaminated Rivers in the 21st Century Using Geochemical and Isotopic Tracers.* Minerals, 2013. **3**(2): p. 192-246.
8. Okabe, T.H., *Bottlenecks in rare metal supply and the importance of recycling - a Japanese perspective.* Transactions of the Institutions of Mining and Metallurgy Section C-Mineral Processing and Extractive Metallurgy, 2017. **126**(1-2): p. 22-32.
9. Satoh, M., *Metal Ion Separation with Functional Adsorbents and Phytoremediation Used as Sustainable Technologies*, in *Applied Environmental Materials Science for Sustainability*. 2017. p. 284-312.
10. Dai, Q.L., et al., *Solution processed MnBi-FeCo magnetic nanocomposites.* Nano Research, 2016. **9**(11): p. 3222-3228.
11. Felez, M.R., A.A. Coelho, and S. Gama, *Magnetic properties of Mn3-xFexSn compounds with tuneable Curie temperature by Fe content for thermomagnetic motors.* Journal of Magnetism and Magnetic Materials, 2017. **444**: p. 280-283.
12. Galizia, P., et al., *Easy batch-scale production of cobalt ferrite nanopowders by two-step milling: Structural and magnetic characterization.* Materials & Design, 2017. **130**: p. 327-335.
13. Mix, T., et al., *Alloying with a few atomic percent of Ga makes MnAl thermodynamically stable.* Acta Materialia, 2017. **128**: p. 160-165.

14. Scheibel, F., et al., *Room-temperature five-tesla coercivity of a rare-earth-free shell-ferromagnet.* Applied Physics Letters, 2017. **110**(19).
15. Zhang, Y.M., G.J. Miller, and B.P.T. Fokwa, *Computational Design of Rare-Earth-Free Magnets with the Ti3Co5B2-Type Structure.* Chemistry of Materials, 2017. **29**(6): p. 2535-2541.
16. Zheng, X.M., et al., *Fabrication and magnetic properties of novel rare-earth-free Fe-Mn-Bi-P thin films by one-step electrodeposition.* Thin Solid Films, 2017. **638**: p. 400-405.
17. Anand, K., J.J. Pulikkotil, and S. Auluck, *Effects of inter-site chemical disorder on the magnetic properties of MnBi.* Journal of Magnetism and Magnetic Materials, 2014. **363**: p. 18-20.
18. DeBoeck, J., et al., *Ferromagnetic Mn-based thin films with perpendicular magnetization on semiconductors.* Physica Scripta, 1996. **T66**: p. 183-189.
19. Dubenko, I., et al., *Magnetocaloric effects in Ni-Mn-X based Heusler alloys with X = Ga, Sb, In.* Journal of Magnetism and Magnetic Materials, 2009. **321**(7): p. 754-757.
20. Jungwirth, T., et al., *Systematic Study of Mn-Doping Trends in Optical Properties of (Ga,Mn)As.* Physical Review Letters, 2010. **105**(22).
21. Ly, V., et al., *Low-temperature phase MnBi compound: A potential candidate for rare-earth free permanent magnets.* Journal of Alloys and Compounds, 2014. **615**: p. S285-S290.
22. Mang, B.W., et al., *On dynamics of grain alignment during alloy solidification under applied magnetic field.* Acta Metallurgica Sinica, 2004. **40**(6): p. 604-608.
23. Lu, Q.M., et al., *Intrinsic magnetic properties of single-phase Mn1+xGa (0 < x < 1) alloys.Scientific Reports, 2015.***5** (17086).
24. Shang, C.H., et al., *Magnetic behavior of MnBi0.47Al0.15 alloy films.* Journal of Applied Physics, 1997. **81**(8): p. 5662-5664.
25. Suzuki, K.Z., et al., *Perpendicular magnetic tunnel junction with a strained Mn-based nanolayer.* Scientific Reports, 2016. **6**.
26. Wei, J.Z., et al., *tau-MnAl with high coercivity and saturation magnetization.* Aip Advances, 2014. **4**(12).
27. Liu, Z.W., et al., *Phase transitions and hard magnetic properties for rapidly solidified MnAl alloys doped with C, B, and rare earth elements.* Journal of Materials Science, 2012. **47**(5): p. 2333-2338.
28. Poudyal, N., et al., *Processing of MnBi bulk magnets with enhanced energy product.* Aip Advances, 2016. **6**(5).
29. Rial, J., et al., *Application of a novel flash-milling procedure for coercivity development in nanocrystalline MnAl permanent magnet powders.* Journal of Physics D-Applied Physics, 2017. **50**(10).
30. Christopher, N.R., et al., *Appreciable Magnetic Moment and Energy Density in Single-Step Normal Route Synthesized MnBi.* Journal of Superconductivity and Novel Magnetism, 2013. **26**(11): p. 3161-3165.
31. Cui, J., et al., *Effect of composition and heat treatment on MnBi magnetic materials.* Acta Materialia, 2014. **79**: p. 374-381.
32. Kavita, S., et al., *On the temperature dependent magnetic properties of as-spun Mn-Bi ribbons.* Journal of Magnetism and Magnetic Materials, 2015. **377**: p. 485-489.
33. Nguyen, P.K., S. Jin, and A.E. Berkowitz, *Unexpected Magnetic Domain Behavior in LTP-MnBi.* Ieee Transactions on Magnetics, 2013. **49**(7): p. 3387-3390.
34. Nguyen, V.V., et al., *Novel processing of high-performance MnBi magnets.* Materials Research Express, 2014. **1**(3).
35. Yang, Y.B., et al., *Temperature dependences of structure and coercivity for melt-spun MnBi compound.* Journal of Magnetism and Magnetic Materials, 2013. **330**: p. 106-110.
36. Zhang, D.T., et al., *Crystal structure and magnetic properties of MnxBi100-x (x=48, 50, 55 and 60) compounds.* Journal of Magnetism and Magnetic Materials, 2012. **324**(11): p. 1877-1890.
37. Cespedes, E., et al., *High coercive LTP-MnBi for high temperature applications: From isolated particles to film-like structures.* Journal of Alloys and Compounds, 2017. **729**: p. 1156-1164.
38. Hozumi, T., et al., *Magnetic and structural properties of MnBi multilayered thin films.* Journal of Applied Physics, 2014. **115**(17).
39. Kempter, K. and E. Bayer, *CURIE-TEMPERATURE AND PHASE-STABILITY OF MNBI FILMS EXPOSED TO LASER PULSES OF VARIABLE DURATION.* Ieee Transactions on Magnetics, 1976. **12**(2): p. 62-65.
40. Li, B., et al., *The structural and magnetic properties of MnBi and exchange coupled MnBi/Fe films.* Journal of Magnetism and Magnetic Materials, 2014. **372**: p. 12-15.
41. Zhou, D., et al., *Preparation of Highly Textured Bi and MnBi Films by the Pulsed Laser Deposition Method.* Chinese Physics Letters, 2015. **32**(12).
42. Kanari, K., et al., *Processing of magnetically anisotropic MnBi particles by surfactant assisted ball milling.* Journal of Magnetism and Magnetic Materials, 2017. **426**: p. 691-697.
43. Kneller, E.F. and R. Hawig, *THE EXCHANGE-SPRING MAGNET - A NEW MATERIAL PRINCIPLE FOR PERMANENT-MAGNETS.* Ieee Transactions on Magnetics, 1991. **27**(4): p. 3588-3600.
44. Nguyen, T.X., et al., *Preparation and Magnetic Properties of MnBi/Co Nanocomposite Magnets.* Journal of Electronic Materials, 2017. **46**(6): p. 3359-3366.
45. Gandha, K., et al., *High Energy Product Developed from Cobalt Nanowires.* Scientific Reports, 2014. **4**.
46. Moon, K.W., et al., *Synthesis and Magnetic Properties of MnBi(LTP) Magnets With High-Energy Product.* Ieee Transactions on Magnetics, 2014. **50**(11).
47. Nguyen, V.V., et al., *High-Performance MnBi Alloy Prepared Using Profiled Heat Treatment.* Ieee Transactions on Magnetics, 2014. **50**(12).
48. Nguyen, V.V. and T.X. Nguyen, *An Approach for Preparing High-Performance MnBi Alloys and Magnets.* Journal of Electronic Materials, 2017. **46**(6): p. 3333-3340.
49. Williams, H.J., et al., *MAGNETIC WRITING ON THIN FILMS OF MNBI.* Journal of Applied Physics, 1957. **28**(10): p. 1181-1184.
50. Yin, F.X., et al., *Sintering formation of low temperature phase MnBi and its disordering in mechanical milling.* Journal of Materials Science & Technology, 1996. **12**(5): p. 335-341.

51. Zhang, W.Y., et al., *High-energy-product MnBi films with controllable anisotropy.* Physica Status Solidi B-Basic Solid State Physics, 2015. **252**(9): p. 1934-1939.
52. Guo, X., Z. Altounian, and J.O. Stromolsen, *FORMATION OF MNBI FERROMAGNETIC PHASES THROUGH CRYSTALLIZATION OF THE AMORPHOUS PHASE.* Journal of Applied Physics, 1991. **69**(8): p. 6067-6069.
53. Myagkov, V.G., et al., *High Rotatable Magnetic Anisotropy in MnBi Thin Films.* Jetp Letters, 2017. **105**(10): p. 651-656.
54. Yoshida, K. and Y. Fujii, *Formation of new Bi similar to Mn alloy phases in vacuum deposited films and their structure determinations by electron microscopy*. Electron, ed. A. Kirkland and P.D. Brown. 1998. 645-651.
55. Andresen, A.F., Engebret.Je, and J. Refsnes, *NEUTRON-DIFFRACTION INVESTIGATIONS ON QUENCHED MNBI AND MNBI0.9SB0.1.* Acta Chemica Scandinavica, 1972. **26**(1): p. 175-&.
56. Chen, D., R.L. Aagard, and T.S. Liu, *MAGNETO-OPTIC PROPERTIES OF QUENCHED THIN FILMS OF MNBI AND OPTICAL MEMORY EXPERIMENTS.* Journal of Applied Physics, 1970. **41**(3): p. 1395-&.
57. Myagkov, V.G., et al., *Structural and magnetic features of solid-phase transformations in Mn/Bi and Bi/Mn films.* Jetp Letters, 2016. **103**(4): p. 254-259.
58. Chang, H.W., et al., *Effect of magnetic field on the structure and magnetic properties of pulse-laser-deposited FePt films.* Journal of Alloys and Compounds, 2014. **584**: p. 148-151.
59. Constantinescu, C., et al., *Optical, morphological and thermal behaviour of NdFeB magnetic thin films grown by radiofrequency plasma-assisted pulsed laser deposition.* Current Applied Physics, 2013. **13**(9): p. 2019-2025.
60. Constantinescu, C., et al., *Thin films of NdFeB deposited by PLD technique*, in *Advanced Laser Technologies 2006*, D.C. Dumitras, M. Dinescu, and V.I. Konov, Editors. 2007.
61. Constantinescu, C., et al., *Thin films of NdFeB deposited by PLD technique.* Applied Surface Science, 2007. **253**(19): p. 8192-8196.
62. Golovchanskiy, I.A., S.A. Fedoseev, and A.V. Pan, *Quantitative model for tunable microstructure in magnetic FePt thin films by pulsed laser deposition.* Journal of Physics D-Applied Physics, 2013. **46**(21).
63. Mokhtari, P., et al., *Microstructure and Magnetic Properties of FePt Thin Films on SiO2/Si (100) and Si Substrates Prepared Under External Magnetic Field.* Journal of Superconductivity and Novel Magnetism, 2017. **30**(7): p. 1949-1961.
64. Nakano, M., et al., *Enhancement in (BH)(max) of PLD-made isotropic Nd-Fe-B thick film magnets deposited on Si substrates.* Aip Advances, 2017. **7**(5).
65. Wang, Y., et al., *Elimination of impurity phase formation in FePt magnetic thin films prepared by pulsed laser deposition.* Applied Surface Science, 2014. **288**: p. 381-391.
66. Ito, M., et al., *Magnetic properties and structure of low temperature phase MnBi with island structure.* Aip Advances, 2017. **7**(5).
67. Moon, H., et al., *Layer-number dependence of the magnetic properties of MnBi films.* Applied Surface Science, 2017. **420**: p. 618-624.
68. Sun, M.Y., et al., *Effect of oxidation on perpendicular magnetic behavior of MnBi thin films.* Journal of Alloys and Compounds, 2016. **672**: p. 59-63.
69. Inpasalini, M.S., et al., *Influence of magnetic ion doping on structural, optical, magnetic and hyperfine properties of nanocrystalline SnO2 based dilute magnetic semiconductors.* Journal of Materials Science-Materials in Electronics, 2017. **28**(4): p. 3285-3292.
70. Singh, A.K., et al., *Influence of antisite disorders on the magnetic properties of double perovskite Nd2NiMnO6.* Solid State Communications, 2016. **242**: p. 74-78.
71. Verma, K.C. and R.K. Kotnala, *Multiferroic approach for Cr, Mn, Fe, Co, Ni, Cu substituted BaTiO3 nanoparticles.* Materials Research Express, 2016. **3**(5).
72. Zhang, W.F., et al., *Tetraazacalix 2 arence 2 triazine Coated Fe3O4/SiO2 Magnetic Nanoparticles for Simultaneous Dispersive Solid Phase Extraction and Determination of Trace Multitarget Analytes.* Analytical Chemistry, 2016. **88**(21): p. 10523-10532.
73. Lopez-Ortega, A., et al., *Applications of exchange coupled bi-magnetic hard/soft and soft/hard magnetic core/shell nanoparticles.* Physics Reports-Review Section of Physics Letters, 2015. **553**: p. 1-32.
74. Lam, N.M., et al., *Fabrication of Mn-Bi Nanoparticles by High Energy Ball Milling.* Materials Transactions, 2015. **56**(9): p. 1394-1398.
75. Rao, N.V.R., et al., *Fabrication of anisotropic MnBi nanoparticles by mechanochemical process.* Journal of Alloys and Compounds, 2014. **586**: p. 349-352.
76. Xu, X., et al., *Magnetic self-assembly for the synthesis of magnetically exchange coupled MnBi/Fe-Co composites.* Journal of Solid State Chemistry, 2015. **231**: p. 108-113.
77. Chwastek, K., *Description of Henkel plots by the magnetization-dependent Jiles–Atherton model.* Journal of Magnetism and Magnetic Materials, 2010. **322**(2): p. 214-217.
78. Khlopkov, K., et al., *Local texture in Nd-Fe-B sintered magnets with maximised energy density.* Journal of Alloys and Compounds, 2004. **365**(1-2): p. 259-265.
79. Li, X.H., et al., *Novel Bimorphological Anisotropic Bulk Nanocomposite Materials with High Energy Products.* Advanced Materials, 2017. **29**(16).
80. Huang, E.Y. and M.H. Kryder, *L1(0)-Ordered MnAl Thin Films With High Perpendicular Magnetic Anisotropy Using TiN Underlayers on Si Substrates.* Ieee Transactions on Magnetics, 2015. **51**(11).
81. Shao, Z.Y., et al., *One step preparation of pure tau-MnAl phase with high magnetization using strip casting method.* Aip Advances, 2017. **7**(5).
82. Jimenez-Villacorta, F., et al., *Magnetism-Structure Correlations during the epsilon ->tau Transformation in Rapidly-Solidified MnAl Nanostructured Alloys.* Metals, 2014. **4**(1): p. 8-19.
83. Wiezorek, J.M.K., et al., *Grain Boundary Mediated Displacive-Diffusional Formation of tau-Phase MnAl.* Metallurgical and Materials Transactions a-Physical Metallurgy and Materials Science, 2011. **42A**(3): p. 594-604.
84. Bittner, F., et al., *The impact of dislocations on coercivity in L1(0)-MnAl.* Journal of Alloys and Compounds, 2017. **704**: p. 528-536.

85. Janotova, I., et al., *Phase analysis and structure of rapidly quenched Al-Mn systems.* Journal of Alloys and Compounds, 2017. **707**: p. 137-141.
86. Matsushita, Y., et al., *L1(0) Stacked Binaries as Candidates for Hard-Magnets: FePt, MnAl and MnGa.* Annalen Der Physik, 2017. **529**(8).
87. Huang, E.Y. and M.H. Kryder, *Fabrication of MnAl thin films with perpendicular anisotropy on Si substrates.* Journal of Applied Physics, 2015. **117**(17).
88. Nie, S.H., et al., *Structural characterization and magnetic properties of perpendicularly magnetized MnAl films grown by molecular-beam epitaxy.* Acta Physica Sinica, 2013. **62**(17).
89. Oogane, M., et al., *L1(0)-ordered MnAl thin films with high perpendicular magnetic anisotropy.* Japanese Journal of Applied Physics, 2017. **56**(8).
90. Zhu, L.J., L. Brandt, and J.H. Zhao, *Engineering the polar magneto-optical Kerr effect in strongly strained L1(0)-MnAl films.* Journal of Physics D-Applied Physics, 2016. **49**(41).
91. Chaturvedi, A., R. Yaqub, and I. Baker, *Microstructure and Magnetic Properties of Bulk Nanocrystalline MnAl.* Metals, 2014. **4**(1): p. 20-27.
92. Zeng, Q., et al., *Structural and magnetic properties of nanostructured Mn-Al-C magnetic materials.* Journal of Magnetism and Magnetic Materials, 2007. **308**(2): p. 214-226.
93. Thielsch, J., F. Bittner, and T.G. Woodcock, *Magnetization reversal processes in hot-extruded tau-MnAl-C.* Journal of Magnetism and Magnetic Materials, 2017. **426**: p. 25-31.
94. Cui, Y.S., et al., *Epitaxial tau phase MnAl thin films on MgO (001) with thickness-dependent magnetic anisotropy.* Journal of Applied Physics, 2011. **110**(10).
95. Hosoda, M., et al., *Fabrication of L1(0)-MnAl perpendicularly magnetized thin films for perpendicular magnetic tunnel junctions.* Journal of Applied Physics, 2012. **111**(7).
96. Saruyama, H., et al., *Fabrication of L1(0)-Ordered MnAl Films for Observation of Tunnel Magnetoresistance Effect.* Japanese Journal of Applied Physics, 2013. **52**(6).
97. Fischer, G.A. and M.L. Rudee, *Effect of magnetic annealing on the tau-phase of MnAl thin films.* Journal of Magnetism and Magnetic Materials, 2000. **213**(3): p. 335-339.
98. Badawi, A., et al., *Enhancement of the optical and mechanical properties of chitosan using Fe2O3 nanoparticles.* Journal of Materials Science-Materials in Electronics, 2017. **28**(15): p. 10877-10884.
99. Gobi, N., et al., *Infusion of Graphene Quantum Dots to Create Stronger, Tougher, and Brighter Polymer Composites.* Acs Omega, 2017. **2**(8): p. 4356-4362.
100. Khabibullin, A., et al., *Injectable Shear-Thinning Fluorescent Hydrogel Formed by Cellulose Nanocrystals and Graphene Quantum Dots.* Langmuir, 2017. **33**(43): p. 12344-12350.
101. Aziz, S.B., O.G. Abdullah, and M.A. Rasheed, *A novel polymer composite with a small optical band gap: New approaches for photonics and optoelectronics.* Journal of Applied Polymer Science, 2017. **134**(21).
102. Ilawe, N.V., M.B. Oviedo, and B.M. Wong, *Real-Time Quantum Dynamics of Long-Range Electronic Excitation Transfer in Plasmonic Nanoantennas.* Journal of Chemical Theory and Computation, 2017. **13**(8): p. 3442-3454.
103. Jeon, S., et al., *Surface functionalized magnetic nanoparticles shift cell behavior with on/off magnetic fields.* Journal of Cellular Physiology, 2018. **233**(2): p. 1168-1178.
104. Hawkins, S.A., et al., *Tensile properties and electrical conductivity of epoxy composite thin films containing zinc oxide quantum dots and multi-walled carbon nanotubes.* Carbon, 2017. **115**: p. 18-27.
105. Velusamy, T., et al., *Ultra-small CuO nanoparticles with tailored energy-band diagram synthesized by a hybrid plasma-liquid process.* Plasma Processes and Polymers, 2017. **14**(7).
106. Su, K.P., et al., *Effect of milling on the structure and magnetic properties in Mn54Al46 flakes prepared by surfactant-assisted ball milling.* Materials Characterization, 2016. **114**: p. 263-266.
107. Shen, J., J. Li, and S.Q. Ren, *Metal-redox for MnAl-Based ternary magnetic nanocrystals.* Rsc Advances, 2016. **6**(48): p. 41781-41784.
108. Meng, K.K., et al., *Anomalous Hall effect and spin-orbit torques in MnGa/IrMn films: Modification from strong spin Hall effect of the antiferromagnet.* Physical Review B, 2016. **94**(21).
109. Ranjbar, R., et al., *Current-induced spin-orbit torque magnetization switching in a MnGa/Pt film with a perpendicular magnetic anisotropy.* Japanese Journal of Applied Physics, 2016. **55**(12).
110. Feng, J.N., et al., *Magnetic Properties and Coercivity of MnGa Films Deposited on Different Substrates.* Journal of Materials Science & Technology, 2017. **33**(3): p. 291-294.
111. Meng, K.K., et al., *Modulated switching current density and spin-orbit torques in MnGa/Ta films with inserting ferromagnetic layers.* Scientific Reports, 2016. **6**.
112. Ono, A., et al., *Ultrathin films of polycrystalline MnGa alloy with perpendicular magnetic anisotropy.* Applied Physics Express, 2017. **10**(2).
113. Zhu, L.J., et al., *Tailoring magnetism of multifunctional MnxGa films with giant perpendicular anisotropy.* Applied Physics Letters, 2013. **102**(13).
114. Arins, A.W., et al., *Structure and Magnetism of MnGa Ultra-Thin Films on GaAs(111)B.* Ieee Transactions on Magnetics, 2013. **49**(12): p. 5595-5598.
115. Zhu, L.J. and J.H. Zhao, *Perpendicularly magnetized MnxGa films: promising materials for future spintronic devices, magnetic recording and permanent magnets.* Applied Physics a-Materials Science & Processing, 2013. **111**(2): p. 379-387.
116. Hasegawa, K., et al., *Material dependence of anomalous Nernst effect in perpendicularly magnetized ordered-alloy thin films.* Applied Physics Letters, 2015. **106**(25).
117. Ma, Q.L., et al., *Interface tailoring effect on magnetic properties and their utilization in MnGa-based perpendicular magnetic tunnel junctions.* Physical Review B, 2013. **87**(18).
118. Mandru, A.O., et al., *Heteroepitaxial growth and surface structure of L1(0)-MnGa(111) ultra-thin films on GaN(0001).* Applied Physics Letters, 2013. **103**(16).
119. Lee, H., et al., *Ferromagnetic MnGaN thin films with perpendicular magnetic anisotropy for spintronics applications.* Applied Physics Letters, 2015. **107**(3).

120. Zhao, S.Q. and T. Suzuki, *Magnetic and structural properties of Mn-Ga thin films.* Aip Advances, 2016. **6**(5).
121. Jamer, M.E., et al., *Magnetic properties and large coercivity of MnxGa nanostructures.* Journal of Magnetism and Magnetic Materials, 2014. **358**: p. 259-262.